Sea level controls on the provenance of fine-grained sediments in the Xisha Trough, northwestern South China Sea over the last ~30 ka

Qiang Zhang[1,2], George E.A. Swann[2], Jianguo Liu[1], Weijian Gao[1,3], Zhenang Cui[4], Gang Li[1], Xuan Zhao[1,3], Wei Li[1]*

[1]*CAS Key Laboratory of Ocean and Marginal Sea Geology, South China Sea Institute of Oceanology, Chinese Academy of Sciences, Guangzhou 510301, China*

[2]*School of Geography, University of Nottingham, University Park, Nottingham, NG7 2RD, UK*

[3]*University of Chinese Academy of Sciences, Beijing 100049, China*

[4]*Sanya Geology Institute of South China Sea, Guangzhou Marine Geological Survey, Sanya 572025, China*

* Correspondence: Wei Li (wli@scsio.ac.cn)

The Xisha Trough situated in the northwestern South China Sea (SCS), plays a pivotal role in transporting sediments from the Red River into the deep-sea basin of the SCS, and thus is a critical place to examine variations in source-to-sink process of the Red River-derived sediments associated with past climate and oceanography changes. In this study, we analyzed clay minerals, grain size composition, and specific XRF core scanning elements of sediment core XT-1, retrieved from the northern slope of the Xisha Trough, to assess changes in sediment provenance and their primary influencing factors in the studied area over the last ~30 ka. The results show that clay minerals are primarily composed of illite+chrolite with a mean of 89%, followed by kaolinite with a mean of 9%; smectite occurs as a minor component. The mean grain size and XRF core scanning elements exhibit a three-phase change that corresponds well to variations in sediment source since the last glacial period. Over the last 29.8 ka, sea level fluctuations are the primary factor controlling changes in provenances and their contributions in the northern slope of the Xisha Trough. During the last glacial from 29.8 to 20.2 ka with lower sea levels, both the Red River and Taiwan were the primary contributors of fine-grained sediments in the lower continental slope of the Xisha Trough. However, with marine transgressions from the last deglaciation, Taiwan gradually became the dominant source of fine-grained sediments, followed by the Red River. Additionally, during the Last Glacial Maximum and the early to middle Holocene periods, the strengthened deep-water current (DWC) and East Asian summer monsoon, respectively, exerted strong impacts on the contribution of Taiwanese sediments to the Xisha Trough. The changing pattern of primary provenance in the studied core is roughly in line with those observed in the northern SCS, while differing from those in the southern regions of the western Xisha Trough. This discrepancy is likely caused by varying influences of the DWC on these regions.

Key words: Xisha Trough, clay minerals, provenance, Taiwan, Red River, sea level

1. Introduction

As the largest semi-enclosed marginal sea in the Western Pacific, the South China Sea (SCS) receives around 700 million tons (Mt) of sediment annually from surrounding rivers and islands (Milliman and Famsworth, 2011), preserving valuable information regarding the evolution of East Asian monsoons, regional tectonic activities, and paleoceanographic changes within its sediments (e.g. Wang et al., 1995; Clift et al., 2002, 2014; Liu et al., 2003a, 2007a, 2012a, 2016a; Wan et al., 2007, 2010). Since the sediments of the SCS are generally derived from diverse sources and are influenced by multiple factors, a comprehensive understanding of the composition, source and transportation process of these sediments is crucial for assessing past changes in the depositional patterns and dynamic conditions within the SCS, as well as their relationships with the paleoclimate, sea-level and current changes (Liu et al., 2016a).

In recent decades, extensive research has been carried out on the sediment source-sink process in the SCS (e.g. Liu et al, 2007b, 2008, 2010a, 2010b, 2013, 2016; Shao et al., 2009; Wei et al., 2012; Li et al., 2015; Cao et al., 2019; Cai et al, 2020), and its changes on various timescales (e.g. Steinke et al., 2003, 2008; Liu et al., 2003a, 2007c, 2010c, 2012a, 2016, 2017; Wan et al., 2007, 2010; Clift et al., 2014). By using datasets of clay mineral assemblages, geochemical elements and Sr-Nd isotopes, the primary and end-member sources for modern sediments in primary regions of the SCS have been well-defined (e.g. Liu et al., 2007b, 2009, 2010a, 2010b, 2013; Shao et al., 2009; Wei et al., 2012). It has been recognized that Taiwan Island, the Pearl River, the Red River, Luzon Island, and Hainan Island are the major contributors of modern sediments in the northern SCS (Liu et al., 2007b; 2010a, 2010b, 2013, 2016a), and the relative contributions of these sources to sediment deposition in the northern SCS are closely related to factors such as the river discharge, climate conditions in the source areas and current systems in the SCS (Liu et al., 2016a). During the Quaternary, changes in terrigenous materials derived from different provenances in the northern SCS showed noticeable glacial-interglacial periodicities, primarily driven by fluctuations in surface currents related to the East Asian monsoon (EAM) (Liu et al., 2003a, 2003b). However, both long-term records and high-resolution sediment cores have also revealed significant temporal and spatial variations in clay mineral composition and depositional patterns that do not correspond to glacial-interglacial cycles along the continental slope of the northern SCS (Boulay et al., 2005; Liu et al., 2010c, 2017). These phenomena were attributed to changes in the relative influences of various sediment sources due to sea-level controlled alterations in the land-sea configuration, river reorganizations on the exposed continental shelf, varying influences of currents at different water depths and changes in current transport ability caused by fluctuations in monsoon strength (Liu et al., 2010c, 2017).

The Xisha Trough (XT) is a primary conduit for transporting sediments from the Red River into the deep-sea basin of the SCS, and thus serves as a critical place for the study of source-to-sink and sedimentation processes related to climate changes in the northwestern SCS. However, until now limited attention has

been paid to past changes in sediment sources and deposition especially in the middle and eastern parts of the Xisha Trough which are connected to the deep basin of the SCS. Some studies suggest that during the Holocene with high sea level, sediments from the Red River were predominantly sequestered in the estuary and on the shelf of the Gulf of Tonkin (e.g. Tanabe et al., 2003, 2006; Ge et al., 2019), and only a small proportion of these sediments were transported to the continental slope and deep water region of the Xisha Trough due to the obstructive effect of Hainan Island (Clift et al., 2008; Shao et al., 2009). Nevertheless, mineralogical and geochemical evidence from the western Xisha Trough indicates that the Red River has been a significant source of sediment supply to the northwestern slope of the SCS and the Xisha Trough during the Holocene (Wan et al., 2015) and even since the middle MIS 3 (Li et al., 2019, 2022). In addition, although Holocene fine-grained sediments from Taiwan and the Pearl River can be transported to the eastern continental shelf of Hainan by coast currents (Tian et al., 2015), their contribution to the sediments on the lower slope of the Xisha Trough is generally considered minimal due to the limited influence of southwestward deep-water current (DWC), which is the primary dynamic for the transport of Tai Wan- and Pearl River-derived sediments to the deep-water regions of the northwestern SCS (Liu et al., 2013, Cai et al., 2020). Clay mineral data from sediment traps and in-situ current data measurements in the Xisha Trough suggest that detrital fine particles in the water column of the Xisha Trough predominantly consisted of high contents of illite and chlorite, and thus concluded that these fine-grained particles were mainly transported from Taiwan by the DWC, with a subsequent contribution from the Red River (Liu et al., 2014a). Whereas, Cai et al., (2020) proposed that although Taiwan made some contributions to the modern sediments on the northwestern slope of the SCS, during the glacial period sediments on the northwestern slope were mainly derived from the paleo-Red River due to the reduced distance between the river mouth and sediment sink, as evidenced by clay mineral and Sr-Nd isotope records in the western Xisha Trough.

During the last glacial period, the decrease in sea level caused noticeable alterations in the land-ocean distribution and thus transport distances of fluvial sediments to the SCS (Steinke et al., 2003, 2008). Specifically, the estuaries of both the Red River and Pearl River migrated towards the outer shelf as the sea level dropped, potentially leading to a substantial increase in sediment transport from these rivers to the SCS (e.g. Liu et al., 2010c, 2016b; Li et al., 2019; Cai et al., 2020). Therefore, it is worth examining whether sea level change contributed to alterations in the transportation of Red River and Pearl River sediments to the Xisha Trough. Additionally, it has been suggested that the DWC experienced a strengthening during the Last Glacial Maximum (LGM) compared to the Holocene (Zheng et al., 2016). Since modern Taiwanese sediments were primarily transported to the northwestern SCS by the DWC (Liu et al., 2014a), it is essential to investigate how sediment composition and deposition in the Xisha Trough responded to changes in the DWC, which would provide valuable insights into the contribution of Taiwan-sourced sediments to the northwestern SCS and its relationships with the DWC.

Clay minerals, as typical weathering products on the Earth's surface, represent a significant component of marine sediments and can be semi-quantitatively analyzed as mineralogical particles to assess terrigenous input (Chamley, 1989). Therefore, they have been widely used to determine the provenance of terrigenous sediments and the transport pathways in the ocean, due to their close relationships with climate conditions in the source regions, as well as the sediment transportation and deposition process in the oceans (Liu et al., 2016a). In this study, we aim to: 1) analyze variations in clay minerals in the sediments from the lower continental slope of the Xisha Trough over the past ~30 ka, 2) determine the primary provenance of fine-grained sediments and estimate sediment contributions from various source areas, and 3) identify the primary factors contributing to variations in sediment provenance and sedimentation in the northwestern slope of the SCS based on the combined data of the clay mineralogy, grain size composition, and XRF core scanning elements.

2. Regional setting

The Xisha Trough, located in the northwestern SCS, is a failed Cenozoic rift with water depths ranging from approximately 1,500 m in the western part to around 3,400 m in the eastern part (Liu and Wu, 2006; Lei et al., 2020). It is bordered by the Qiongdongnan Basin to the west, Northwest Sub-Basin to the east, Shehu Rise to the north, and Xisha Islands to the south (Figure 1a). Based on its morphological characteristics and extension direction, the Xisha Trough can be divided into three parts as follows: the eastern Xisha Trough, located to the east of 112°40' E with the extension in a NEE direction, middle part of the Xisha Trough, situated between 112°40' E and 111°40' E with an approximate east-west direction, and the western Xisha Trough, found to the west of 111°40' E with a NE direction (Liu and Wu, 2006).

In the SCS, the ocean circulation, which is the primary driving force for the sediment transport and deposition, varies with water depths. Although the intermediate circulation has not been fully understood (Chen, 2005; Zhu et al., 2019), it is widely accepted that the surface circulation in the SCS affects the water layer generally above ~350 m in depth, and is primarily influenced by the distinct seasonal monsoon winds induced by differential heating between the NW Pacific and the Asian land-mass (Fang et al., 1998; Wang and Li, 2009).

During winter, the surface current flows southwestward driven by the northeast monsoon, while in summer, it flows in the opposite direction under the effect of the southwestern monsoon (Shaw and Chao, 1994; Fang et al., 1998, 2012) (Figure 1a). During the Quaternary, the EAM-driven surface current had strong impacts on the distribution and contents of different clay components in the SCS. Consequently, several proxies based on sedimentary records, such as clay minerals, have been proposed to indicate the evolution of the EAM (Liu et al., 2003a, 2007c). The Kuroshio Current from the western Pacific intrudes into the northern SCS through the Luzon Strait and transports water in the upper 300-500 m westward along

the northern continental slope of the SCS (Shaw and Chao, 1994; Nan et al., 2015), mainly impacting the water mass properties and sedimentation processes on the shelf/slope region in the northern SCS (Xue et al.., 2004; Liu et al., 2011), as well as the transport of smectite from Luzon Island to the northern SCS (Liu et al., 2010b, 2016a).

The DWC in the SCS occurs at depths below ~1,500 m and originates from the Northern Pacific Deep Water that flows into the SCS through the Luzon Strait (Wang et al., 2011; Zhao et al., 2014). After entering the SCS, the DWC initially turns northwestward and then turns southwestward along the continental margins offshore southeast China (Qu et al., 2006; Wang et al., 2018). Although the distribution route of the modern DWC is not fully constrained, it is suggested that the DWC primarily flows from north to south along the edge of the deep basin (Wang et al., 2011; Liu J G et al., 2013), and may not extend into the Xisha Trough nor substantially impact sediment deposition in that region. However, in-situ observations of the current in the western Xisha Trough indicate the presence of the deep-water current for most of the year with a mean velocity of 5–6 cm/s (Liu et al., 2014). Simulation analysis suggests that when the DWC sweeps the SCS northern margins and encounter the Xisha Trough, it splits into three parts, (1) one part flows into the Xisha Trough along its northern slope to the west, (2) the second part flows towards the seamount plateau and generate local circulations, (3) the remaining part of the DWC heads towards to the south and sweeps the eastern margins of the seamount plateau (Chen et al., 2016).

3. Material and Method 3.1 Sample material

Gravity core XT-1 (18o14’35.56’’; 111o41’26.30’’E; water depth of 1803 m) was collected from the northern slope of the middle part of the Xisha Trough in the northwestern SCS (Figure 1a). Specifically, it was obtained from the bank of a submarine canyon indicated by the bathymetric map (Figure 1b), which provided an advantageous location for minimizing disturbances from turbidity current depositions. The core is 3.99 m in length. The uppermost ca. 15 cm of the sediment core comprises brownish-yellow clayey silt, whereas the lower section is dominated by homogeneous and olive gray to dark gray clayey silt enriched with foraminifera. A notable turbidite layer can be observed within the interval from 3.46 to 3.53 m, which may result in a hiatus or sedimentary anomaly below 3.44 m. Therefore, our study primarily focuses on the layers above 3.44 m for sedimentary analysis.

3.2 Radiocarbon dating

A total of 10 samples of the mono-planktonic foraminifera *Globigerinoides ruber* (white) or mixed species of *G*. *ruber* and G*. sacculifer* from core XT-1 were used for accelerator mass spectrometry (AMS) ^{14}C-datings at BETA Lab in the United States, in order to establish the chronostratigraphic framework and estimate linear sedimentation rates for core XT-1. All radiocarbon dates were converted to calendar ages with the

CALIB 8.2.0 software, using the MARINE 20 calibration dataset with a regional ^{14}C reservoir age of ΔR=-149±40 years (Southon et al., 2002).

3.3 XRF core element scanning

The major elements of the sediment core were analyzed at the Key Laboratory of Ocean and Marginal Sea Geology, South China Sea Institute of Oceanology, Chinese Academy of Sciences (CAS), using a GEOTEK Multi-Sensor Core Logger equipped with high-resolution X-ray core scanner. Before the scanning, the surfaces of split cores were smoothed and covered with a thin Ultralene film to avoid contamination of the XRF measurement unit. Measurements were performed at 1 cm intervals with settings of 10 kV and 500 mA to obtain the intensities of elements, which were then converted into the content of each element by the integrated software of Geotek MSCL for the Instrument. The element data detected by the XRF core scanner are presented in relative abundance. To ensure the reliability of the test results, only the element data with values higher than 500ppm were selected for further analysis.

3.4 Grain size analysis

A total of 127 samples were taken with a sampling interval ranging from 2 to 4 cm for the grain size analysis of the terrigenous fraction. These samples were treated with 30% H_2O_2, 10% HCl, and 2 mol/L Na_2CO_3 in a water bath at 80°C to remove organic matter, carbonate and biogenic opal, respectively, and then rinsed three times with deionized H_2O using centrifugation. Prior to the grain size analyses, 10 ml of 0.05molL^{-1} dissolved Sodium hexametaphosphate $(NaPO_3)_6$ was added to ensure the disaggregation of potential aggregates. The sediment grain sizes ranging from 0.02 to 2000 μm were analyzed using the Malvern Mastersizer 2000 at the Key Laboratory of Ocean and Marginal Sea Geology, South China Sea Institute of Oceanology, CAS. The reproducibility exceeds 2% for duplicate samples.

3.5 Clay mineral analysis

127 samples collected from the layers for the grain size analysis were retaken for clay mineral analysis. Clay minerals (<2 μm) in each sample were separated by the settling method based on the Stoke's settling velocity principle. Before the separation process, organic matter and carbonate in sediments were removed from the sediments by treating them with excess 10% hydrogen peroxide (H_2O_2) and 10% acetic acid (CH_3COOH), respectively. Following ethylene glycol solvation for 24 h at 60°C, the clay minerals were analyzed using Standard X-ray diffraction (XRD) on a D8 ADVANCE diffractometer with CuKα radiation (40 kV, 40 mA), at the Key Laboratory of Ocean and Marginal Sea Geology, South China Sea Institute of Oceanology, CAS. The relative percentages of the four clay mineral groups were determined by weighting integrated peak areas of characteristic basal reflections (smectite –17 Å, illite –10 Å, and kaolinite/chlorite –

7 Å) using the Topas-5 software with the empirical factors of Biscaye (1965). The relative proportions of kaolinite and chlorite were calculated from the ratio of 3.57/3.54 Å peak areas.

The crystallinity of clay minerals is an effective measure of the lattice ordering and crystallite size (Biscaye, 1965; Ehrmann, 1998). The illite crystallinity is typically estimated at the full width at half maximum (FWHM) of the illite 10 Å peak (Petschikc et al., 1996; Ehrmann, 1998). Lower values of crystallinity indicate the better crystallinity of illite primarily resulting from physical weathering processes. The illite chemistry index is a parameter to measure the weathering degree of illite, which is estimated using the ratio of 5 Å and 10 Å illite peak areas. Values below 0.4 indicate Fe-Mg-rich illites formed through physically weathering, while those above 0.4 represent Al-rich illites, which are indicative of strong hydrolysis (Ehrmann, 1998; Wan et al., 2008). Therefore, both the illite crystallinity and chemistry index are employed to trace the natures of the weathering processes and climate conditions in the source areas (Ehrmann, 1998; Wan et al., 2008).

3.6 Quantitative analysis of provenances

To assess changes in relative contributions of the potential sediment sources, we employed a method of Liu et al. (2012b, 2013) known as the minimum error between estimated and actual values based on clay mineral data. Firstly, various sediment sources and their compositions of clay minerals (Xij, where i represents the sample numbers from 1 to n, and j denotes the specific clay mineral component from 1 to m) are determined. Secondly, preliminary coefficients are assigned to each source (ωi, where i = 1, 2, ..., n, Σωi = 1). Thirdly, estimated values (Xijωi, *i* = 1, 2, ..., n, j = 1, 2, ..., m) are generated alongside the corresponding actual values (Yj, i=1, 2,..., m). Finally, the coefficients are iteratively adjusted to minimize the error between the estimated values and actual values (Z=ΣXij*ωi-Yj, i=1, 2, ..., n; j=1, 2, ..., m).

In combination with the clay content of sediments, the sediment accumulation rate and relative contribution of clay minerals from different sources, we further estimated the mass accumulation rates (MARs) of different clay mineral components from various provenances. The MAR of each clay mineral component was calculated as follows:

MAR [$g/cm^2/ka$] = (clay content of sediments) [%]
x (relative contribution of specific clay mineral) [%]
x (the density of dried clay minerals) [g. cm-3]
x (sedimentation rate) [$cm. ka^{-1}$].

It is assumed that dried clay minerals with non-swelling layers possess a mean density of 1.99 g/cm^3, as their density typically ranges from 1.52 to 2.46 g/cm^3 (Osipov, 2012).

4 Results

4.1 Age model and sedimentation rate

The age model of sediment core XT-1 was established using 10 AMS ^{14}C age data (Table 1). Based on this, the studied core covers a continuous sedimentary succession spanning the last 29.8 ka BP (Figure 2a). Age determinations for various layers were derived through linear interpolation, assuming a constant sedimentation rate between adjacent median calibrated age points. During the period from 29.8 to 20.1 ka, the sedimentation rate (SR) ranged from 8.3 to 26.9 cm/ka, with a mean SR of 14 cm/ka (Figure 2b). From 20.1 to 11.9 ka, the SR fluctuated between 6.8 and 12.1 cm/ka, averaging at 10.4 cm/ka. In the last 11.9 ka, the SR varied from 6.5 to 14.4 cm/ka, averaging 10.1 cm/ka. The highest mean SR of 26.9 cm/ka occurred between 22.6 to 19.6 ka, coinciding with sea level fluctuations between −120 m and −100 m (Hanebuth et al., 2000; Grant et al., 2014). The sedimentation rate for the studied core was calculated as 12.5 cm/ka during late glacial period (MIS 3-2) and 10.1 cm/ka during the Holocene, approximately consistent with those of sediment cores C7 (13.2 cm/ka and 11.3 cm/ka, respectively) and C120 (12.1 cm/ka and 9 cm/ka) retrieved from the western Xisha Trough (Cai et al., 2020).

4.2 Core scanning elements and grain sizes

In this study, we focus mainly on aluminum (Al), silicon (Si), calcium (Ca), and titanium (Ti) due to their significance role in tracing changes in terrigenous input. Ti is predominantly derived from terrigenous materials, and thus generally varies in accordance with the terrigenous content of the sediment. Ca is typically associated with the carbonate content of the biogenic fraction within the sediments, particularly in the deep-sea environments. Therefore, the natural logarithmic ratio between Ca and Ti can be used to evaluate the relative dilution of biogenic carbonate resulting from terrigenous input (Bahr et al., 2005; Kuhnt et al., 2015), with lower values indicating a higher terrigenous input. In comparison to Si, Al is primarily rich in aluminosilicates of clay-sized particles, while Si can exist as quartz in silt-sized particles, as well as in the form of aluminosilicates. Consequently, the natural logarithmic ratio of Si/Al has been proposed to trace changes in quartz content relative to aluminosilicates in marine sediments, where high values suggest a higher proportion of coarser particles compared to the clay fraction (Calvert et al., 1993; Meckler et al., 2013).

Figure 3 shows the element data of Ca, Ti Al and Si in core XT-1 measured by the XRF core scanner. The contents of these four elements, along with ln-ratios of Ca/Ti and Si/Al, exhibit a nearly synchronous change with varying amplitudes. The content of Ti shows an slightly decreasing trend throughout the core,

while Ca and the ln(Ca/Ti) ratio exhibit an inverse trend with the element Ti, with low values observed before ~13.5 ka, and a distinct increase thereafter. This suggests a greater input of terrigenous materials and a higher dilution of biogenic carbonate before 13.5 ka compared to the interval after 13.5 ka. The contents of Si and Al, along with the ln(Si/Al) ratio, also show a similar pattern of change with an overall decreasing trend, indicating a gradual reduction in the coarse fraction of the sediments during the past 29.8 ka.

The sediments of core XT-1 are predominantly composed of silt and clay, with sand being only a minor component (~1%) (Figure 3a). The silt content ranges from 55% to 71%, averaging at 64%, while the clay faction varies between 28% and 48%, with a mean of 35%. Overall, there is an increasing trend in the clay content during the last 29.8 ka, whereas both the content of silt and mean grain size exhibit a decreasing trend (Figure 3). These findings suggest a decrease in the coarse fraction throughout the studied core, consistent with the changes in coarse fraction inferred from the ln(Si/Al) ratio.

4.3 Changes in clay mineral assemblages

The clay mineral assemblages in core XT-1 primarily consist of illite, chlorite and kaolinite (Figure 4). Illite is the dominant clay mineral with an mean content of 80%, followed by chlorite and kaolinite with mean contents of 9% each. Smectite is present as a minor component with a mean content of 2% (Figure 4). Among the content variations of the four clay minerals, illite and chlorite, kaolinite and smectite exhibit similar variation patterns with positive correlations (Figures 4 and 5). This indicates that illite and chlorite, kaolinite and smectite originate from the same source or share the common transportation mechanism, respectively. Based on the variations in illite/chlorite and kaolinite contents, which showed distinct changes at 20.2 ka and 13.5 ka respectively, changes in clay mineral assemblages can be divided into three intervals from Stages I to III (Figure 4), approximately corresponding to the last glacial period, the last deglaciation and the Holocene, respectively.

During stage I (29.8 to 20.2 ka), the contents of illite and chlorite was relatively low, averaging at 76% and 8% respectively, with noticeable fluctuations from 23 to 20.2 ka (LGM). In contrast, both kaolinite and smectite contents varied greatly with relatively high mean values of 12% and 4% respectively. Subsequently, during stage II (20.2 to 13.5 ka), the illite and chlorite contents showed an overall increasing trend, with relatively stable values (mean=80% and 9%, respectively). Simultaneously, the contents of kaolinite (mean=10%) and smectite (mean=1%) exhibited a decreasing trend. The clay mineral assemblages during stage III (13.5 ka BP to present, Holocene) were characterized by consistently high illite and chlorite contents (averaging at 85% and 11%, respectively), along with a further decrease in the kaolinite content (mean=4%) and almost complete absence of smectite. In the topmost sample of the core, the clay mineral assemblages consisted of 83% illite, 5% kaolinite, 11% chlorite and 1% smectite, which are approximately

consistent with those of suspended particles observed in the water column (82–83% illite, 7–9% kaolinite, 6–8% chlorite and 1– 3% smectite) of the western Xisha Tough (Liu et al., 2014a). Considering the similar changing patterns and the relatively high linear correlation between illite and chlorite (Figure 5), we use illite+chlorite to show their combined change in the subsequent text.

The values of the illite crystallinity in the studied core range from 0.1 to 0.45°△2θ with a mean of 0.24°△2θ and an overall decreasing trend, indicating that illite was well crystalline throughout the core. The illite crystallinity exhibits a relatively high mean value of 0.25°△2θ before 20.2 ka, a moderate mean of 0.2°△2θ from ~20.2 to 13.5 ka, and a low mean value of 0.17°△2θ during the past 13.5 ka (Figure 4). Similar to the illite crystallinity, the illite chemistry index also exhibit an overall decreasing trend throughout the core. It fluctuates between 0.2 and 0.6 with a mean of 0.4 from 29.8 ka to ~20.2 ka, and is relatively stable with a mean of 0.35 from 20.2 ka to 13.5 ka, and averaging at 0.33 duing the last 13.5 ka BP. Both changes in the illite crystallinity and chemistry index may indicate that the source of illite in the studied core gradually shifted to a provenance characterized by strong physical weathering.

5 Discussions

5.1 Source analysis of clay minerals

A detailed understanding of the potential source areas and transport mechanisms of individual clay minerals is fundamental for interpreting the climatic and sedimentary conditions, as well as determining the factors influencing changes in clay mineral records (Gingele et al., 1996; Ehrmann, 1998; Wan et al., 2007; Zhang et al., 2015; Liu Z F et al., 2016). In the entire northern SCS, terrigeous materials primarily comprise continental clastics contributed by the rivers surrounding the SCS, with only a minor contribution of eolian sediments in the northern SCS during the Quaternary (Liu et al., 2003a; Boulay et al., 2005, 2007). Studies on the modern source-to-sink process of sediments in the SCS have demonstrated that Taiwan, South China, Indochina, Hainan Island and Luzon Islands are the primary potential sources of terrigenous input in the northern SCS (Shao et al., 2009; Liu Z F et al., 2010a, 2010b, 2013, 2016a). Based on clay mineralogy of the surface sediment, it has been observed that the provenance of surface sediment in northwestern SCS notably varies from the continental shelf to the slope (Liu et al., 2013; Cai el al., 2020). Sediments deposited in the eastern shelf of Hainan Islands exhibits relatively high amounts of smectite (mean=20%) and kaolinite (mean=19%), which are considered to be derived mainly from Hainan and the South China (Cai et al., 2020). Conversely, sediments in the slope regions have high contents of illite+chlorite (mean=72%) and originate from more complex sediment sources (Liu et al., 2013; Cai et al., 2020). Liu et al., (2013) studied the distribution of clay minerals and rare earth elements in surface sediments of the SCS, and suggested that Taiwan was the predominant contributor of fine-grained sediments on the northern slope of the Xisha Trough, followed by the Red River. However, Cai et al., (2020) proposed that input from the west, including the Red River and Hainan Island were likely the major

provenance of sediment in the western Xisha Trough of the northwestern SCS, with some contributions from the Pearl River and Luzon evidenced by the clay mineralogy and Sr-Nd isotopic composition of sediments.

In core XT-1, the mean content of illite+chlorite throughout the core is approximately 89% (Figure 4), which is significantly higher than that reported in surface sediments from the northwestern slope of the SCS and the surrounding rivers of Indochina and Hainan Island (Liu et al., 2007a, 2007b, 2013; Hu et al., 2014; Cai et al., 2020). However, this observation is well consistent with the findings of suspended particles in the water column of the western Xisha Trough, where a high illite+chlorite content ranging from 88% to 91% was observed (Liu et al., 2014a). These findings suggest that Taiwan is likely the primary contributor to the high illite+chlorite content in the studied core, rather than the Red River or Hainan. Taiwan is the largest source of suspended sediment directly entering the SCS, estimated at approximately 176 Mt per year (Dadson et al., 2003). The clay minerals derived from Taiwanese riverine sediments are predominantly composed of illite+chlorite, averaging approximately 99% (Liu et al., 2008, 2010a, 2014a), and can be transported southwestward along the lower continental slope by the DWC in the northern SCS (Shao et al., 2007; Wan et al., 2010; Liu et al, 2016a). In-situ observations of the current and suspended particles in the water column of the western Xisha Trough have indicated the presence of a stable DWC that flows through the Xisha Trough for much of the year, and can transport modern Taiwanese sediments to the lower continental slope regions of the northwestern SCS (Liu et al., 2014a). This observations is further supported by the numerical simulation results of hydrodynamic and sediment transport processes, which reveal that when the DWC reaches the intersection of the Xisha Trough and the Northwest Sub-Basin, part of it flows into the Xisha Trough along its northern slope towards the west (Chen et al., 2016). Therefore, we suggest that Taiwan is the main source of the high illite+chlorite content observed in the studied core.

The Pearl River in the South China annually transports approximately 84 Mt of terrigenous materials to the SCS (Zhang et al., 2012). The fine-grained particles from the Pearl River are characterized by high kaolinite content (averaging 34%) and illite+chlorite (averaging 65%) due to intensive chemical weathering in the river drainage basin under the background of warm and humid climates (Liu et al., 2007a; Zhang et al., 2012), and it thus is considered an important end-member source for kaolinite in the northern SCS. Although modern sediments from the Pearl River are primarily transported southwestward by the coastal current throughout the year (Liu et al., 2014b), mainly depositing along the continental shelf between the Pearl River delta and Hainan Island (Liu et al., 2013; Li et al., 2015), during glacial periods sediments originating from the Pearl River system could be transported to the outer shelf in the northeastern SCS as the river mouth migrated seawards due to falling sea level (Liu et al., 2010c, 2016a, 2016b, 2017). Subsequently, they may be further delivered to the northwestern SCS by the DWC, becoming an important source of kaolinite in the studied area.

Considering the positive relationship between smectite and kaolinite, it is likely they share a common source or transportation mechanism. However, smectite is nearly absent from fluvial sediments in the Pearl River (Liu et al., 2007b, 2010b). Luzon is the primary source for smecite in the northern SCS, but smectite from Luzon is predominantly deposited in the northeastern SCS, delivered by the northwestward SCS Branch of Kuroshio (Liu et al., 2009, 2016a). Liu et al., (2013) reported that sediments from the area east of Pearl River (EPR) showed a similarly high smectite content (mean=37%) as those from Luzon, which contributed varying amounts of terrigenous input in the northern continental slope since the LGM (Liu et al., 2016b). As smectite was a minor component in the studied core and mainly occurred during the glacial period, similar to kaolinite, we suggest that the smectite in the vicinity of the studied core likely originated from the EPR, and was transported to the northwestern slope by the DWC, along with kaolinite originating from the Pearl River.

The Red River, which flows through the Indochina region, contributes about 130 Mt/year of fluvial sediments to the SCS (Milliman and Syvitski, 1992). Sediments discharged from the Red River are characterized by a relatively high content of illite+chlorite (averaging 79%), and low amount of kaolinite and smectite (averaging 18% and 3%, respectively), resulting from physical erosion under cold and arid climatic conditions in the source regions (Liu et al., 2007a). Although a significant amount of fluvial sediment from the Red River has been sequestered in the Gulf of Tonkin during the Holocene due to high sea levels (Tanabe et al., 2003; Ge et al., 2019), the Red River is still considered an important source of sediments in the northwestern slope and Xisha Trough (Liu et al., 2014a; Wan et al. 2015; Li et al., 2019). During glacial sea-level lowstands, the terrigenous input significantly increased due to the shortened distance between the river mouth and the studied area (Li et al., 2019, Cai et al., 2020), similar to the Pearl River. Consequently, the Red River should be one of the primary sediment sources of the studied area.

Whilst Hainan Island is geographically closer to the studied area, it is not considered to be the primary sediment source for the vicinity of core XT-1. The annual sediment discharge from the major rivers of Hainan is relatively low, with less than 4 Mt / year (Zhang et al., 2013), and these sediments are primarily deposited in the continental shelf of the Hainan Island (Hu et al., 2014; Cai et al., 2020). The fluvial discharge from rivers in the western Hainan Island is mainly deposited in the inner shelf of western Hainan, thus having minimal impacts on marine sediments in the eastern sea area of Hainan Island (Hu et al., 2014; Cai et al., 2020). The fluvial sediments from Hainan Island that could potentially affect the studied area are mainly derived from the rivers in the eastern Hainan. However, these sediments are primarily deposited in the eastern continental shelf of Hainan (Hu et al., 2014; Cai et al., 2020), and consist mainly of kaolinite (51%), with a relatively lower content of chlorite+illite (48%) and a minimal amount of smectite (1%) (Hu et al., 2014). This composition is inconsistent with the clay mineral assemblages observed in core XT-1, which is predominantly composed of illite+chlorite (mean=89%), followed by kaolinite (9%). Furthermore, these sediments exhibit high values of illite chemical index and crystallinity, averaging 0.8 and 0.38, respectively,

due to intense chemical wreathing under the warm and humid climate (Hu et al., 2014). However, the sediments throughout the studied core are characterized by low values of illite chemical index and crystallinity (mean=0.37 and 0.21, respectively) (Figure 4), suggesting that Hainan contributes a negligible amount of clay minerals to the studied area. Additionally, Luzon Island and other distant areas, located thousands of kilometers away from the study site, are also expected to have limited contributions to the sediment source of the northwestern slope in the SCS (Liu et al., 2013).

In order to further examine the provenance of the clay minerals in core XT-1, the clay mineral assemblages throughout the studied core were compared with those of surface sediments from potential provenances mentioned above, using the end-member analysis of clay minerals (Figure 6). The results indicate multiple sources and phased changes of clay minerals within the studied core. Over the past 29.8 ka, Taiwan, the Red River, the Pearl River and the EPR were identified as the primary sources of the clay mineral components in core QND-1. Generally, the samples fell within the range of the Taiwan, Red River, Pearl River, and EPR provenances, with large fluctuations during stage I (29.8-20.2 ka) (Figure 6a). Subsequently, the samples lie mainly between the Taiwan and Red River provenances, with a few samples close to the Pearl River provenance during stage II (20.2-13.5 ka) (Figure 6b), and then become closer to the Taiwan provenance during stage III (13.5 ka to present) (Figure 6c). These findings suggest that the sediments in the sediment core XT-1 represent a mixture of components from Taiwan, the Red River, the Pearl River and the EPR region, with varying contributions from each provenance. During the last glacial period before 20.2 ka, both the Red River and Taiwan were the primary sources of detrital fine-grained sediments in lower continental slope of the Xisha Trough, with some contributions from the Pearl River and the EPR. However, during the last deglaciation (20.2-13.5 ka), the provenance gradually shifted towards Taiwan with an increased contribution from the Pearl River. Eventually, Taiwan became the dominant source for sediments during the Holocene.

The shifts in the provenances of fine-grained sediment in the core XT-1 can be confirmed by variations in the chemical index and crystallinity of illite, which are closely related to the type and intensity of weathering in the source regions. In general, sediments from the Taiwan exhibit a low illite chemistry index and crystallinity due to strong physical weathering caused by an active tectonic setting and high precipitation, with mean values of 0.33 and 0.16, respectively (Liu et al., 2008). Similarly, sediments derived from the Red River also present a low illite chemistry index and crystallinity because of enhanced direct rock erosion within the Red River drainage basin under cold and arid climatic conditions, averaging at 0.4 and 0.2, respectively (Liu et al., 2007a). However, sediments from the Pearl River in the South China are characterized by a high chemistry index and crystallinity of illite due to intensive chemical weathering under subtropical and wet climate conditions, with mean values of 0.62 and 0.3, respectively (Liu et al., 2007a, 2007b). When comparing the illite chemistry and crystallinity data of the studied core with those from potential sources, the results show that most samples are located closer to Taiwan provenance during

the Holocene (13.5-0 ka) (Figure 6c'), mainly between Taiwan and Red River provenances during the last deglacial period (20.2-13.5 ka) (Figure 6b'), and scattering among Taiwan, Red River, and Pearl River provenances during the glacial period (29.8-20.2 ka) (Figure 6a'). These changes indicate a general increase in the contribution of sediments from Taiwan to the studied area, and a gradual decrease in the sediment supply from Red River and Pearl River over the past ~29.8ka, which is consistent with results from the clay mineral composition.

5.2 Controls of changes in provenances and their contributions

The minimum error method of Liu et al. (2012b, 2013), as described in section "2.6 Quantitative analysis of provenances" was employed to estimate the proportion of sediment contributed by each source, assuming that the compositional characteristics of clay minerals from various sources remained relatively stable over time. The clay mineral compositions of the sediment sources derived from the literature, which were used to determine their relative contributions to the Xisha Trough in the northwestern SCS, were recalculated using the method of Biscaye (1965). The resulting mean compositions of clay minerals were as follows: 99% illite+chrolite and 1% kaolinite for Taiwan (19 samples) (Liu et al., 2007b, 2008), 79% illite+chrolite, 18% kaolinite, and 3% smectite for the Red River (39 samples) (Liu et al., 2007a), 65% illite+chlorite, 34% kaolinite and 1% smectite for the Pearl River (7 samples) (Liu et al., 2007a), and 40% illite+chlorite, 23% kaolinite and 37% smectite (35 samples) for the EPR (Liu et al., 2016b).

The estimated results show that Taiwan and the Red River are the primary sediment sources, accounting for a mean of 63% and 26% respectively of the total clay component throughout core XT-1 (Figure 7). In contrast, the Pearl River and the EPR made smaller contributions, averaging 6% and 5% respectively (Figure 7). These findings support the conclusion drawn from the modern observation that Taiwan, despite its greater distance from the studied area, has been the main source of fine-grained sediments on the lower continental slope of the Xisha Trough, followed by the Red River (Liu et al., 2014a). Overall, a three-stage pattern can be discerned in the relative contributions of the four sediment sources (Figure 7). During the glacial period with lower sea levels (29.8 ka to 20.2 ka), the Red River and Taiwan were the primary sediment sources for the studied area, contributing a mean of 37% and 44% respectively, associated with greater amplitude variability. The Pearl River and the EPR contributed a mean of 12% and 7% respectively. As the sea level gradually rose from its lowest level at ~20.2 ka, the contribution of sediments from the EPR became negligible and there was no sediment supply from this source thereafter. During the last deglaciation (20.2 to 13.5 Ka), the relative contributions from Taiwan and the Pearl River increased to a mean of 61% and 14% respectively, with the percentage of the Pearl River' supply reaching its highest mean value. Meanwhile, the contribution of the Red River gradually decreased to a mean of 25% as sea levels rose. In the Holocene period (13.5 ka to present), the relative contribution of the Red River further decreased to a mean of 16%, while Taiwan's contribution increased to a mean of 83% as sea levels

continuously rose. Pearl River contributed only a small amount of sediments, averaging approximately 1% (Figure 7).

In general, changes in the climatic condition (rainfall and temperature) and the lithology in sediment source areas, along with fluctuations in sea level and current system, have substantial impacts on sediment compositions, the discharge of different sources, as well as the transport and deposition of sediment in marginal seas (e.g. Steinke et al., 2003, 2008; Boulay et al., 2005; Liu et al., 2007a, 2016a; Wan et al., 2008, 2015; Yu et al., 2019, 2020). Consequently, these factors may influence the contributions from various sediment provenances. Sedimentary records of the fluvial sediments in and around the SCS suggest that East Asian monsoon (EAM) climate (rainfall and temperature) is the primary driver of changes in chemical weathering intensity, clay mineral composition and sediment discharge from fluvial drainage systems in Inland East Asia during the late Quaternary (Liu et al., 2007c; Li et al., 2022). Although the relationship between the EAM and rainfall during the late Quaternary remains controversial due to regional differences (Sun et al., 2000, 2015; Thomas et al., 2014; Dai et al., 2015; Clemens et al., 2018; Zhao et al., 2020; Lyu et al., 2021), compared to glacial periods, the chemical weathering in East Asia was generally stronger due to more warm and humid climates during interglacial periods induced by the strengthening of the East Asian summer monsoon (EASM) (Guo et al., 2000; Wang et al., 2008; Clift et al., 2014; Li et al., 2022). In addition, the clay mineral composition in terrigenous materials is mainly influenced by the type and intensity of weathering and geological characteristics of the river drainage basin (Wan et al., 2007; Liu et al., 2007a, 2016a; Clift et al., 2014). Illite and chlorite are the primary minerals formed through weak hydrolysis and physical erosion of rocks under cold and arid climatic conditions, while kaolinite is a second secondary mineral indicating strong hydrolysis and intensive chemical weathering in warm and humid climates (Chamley, 1989; Liu et al., 2016a). Therefore, if the sediment composition and contributions from various sources were primarily controlled by the intensity of weathering related to the EAM climate, we would expect a higher content of kaolinite and lower amount of illite+chrolite, associated with corresponding fluxes from their source areas during the Holocene compared to glacial periods. However, the mean content of kaolinite and the mean MARs from its source, the Pearl River, exhibit notably higher values during the LGM than during the Holocene (Figures 4 and 8). Conversely, the mean content of illite+chrolite and the mean MARs of its source, Taiwan, exhibit notably lower values during the LGM than during the Holocene (Figures 4 and 8), contrary to the expected result. This implies that changes in weathering in the source areas controlled by the EAM climate may not be primarily responsible for the observed variations in the clay mineral records and relative contributions from various sources in the studied area.

These findings can also be confirmed by the chemistry index and crystallinity of illite in the studied core. Higher values of the illite chemical index and crystallinity generally indicate stronger chemical weathering under warmer climatic conditions (Gingele et al., 1996; Liu et al., 2016a). However, illite chemical index and crystallinity in the studied core show higher values during the glacial than during the Holocene (Figure 4),

indicating the minor influence of the EAM changes on the clay mineral characteristics and thus the contribution of primary provenances during different periods. These observations suggest that changes in clay minerals in core XT-1 and the relative contributions from various sources may not be caused by varied weathering driven by the EAM climate, but were more likely the result of shifts in sediment sources over the past ~30 ka.

During the Quaternary, global sea levels experienced frequent fluctuations due to cyclic climate changes, leading to significant alterations in the land-sea configuration, sediment source areas and deposition patterns both in the northern and southern regions of the South China Sea (Steinke et al., 2003, 2008; Liu et al., 2010c, 2016a, 2017). When comparing our data with the sea level curve of the past ~ 30 ka, we observed corresponding variations in clay mineral assemblages, sediment grain sizes, and major element compositions in core XT-1 that closely aligned with sea level changes (Figures 3, 7 and 8), which likely influenced the relative contributions from different sediment sources. During the glacial period from 29.8 to ~20.2 ka, when sea levels dropped from −100m to −120m (Grant et al., 2014), both the Red River and the Pearl River showed a slight increasing trend in their relative contributions (mean= 37% and 12%, respectively) and MARs (mean= 4.7 and 3.6 g/cm^2/ka, respectively) (Figures 7 and 8), indicating an enhanced supply of fluvial sediments from these rivers to the slope regions of the northwestern SCS. This observation is in agreement with previous studies suggesting that as sea levels continuously decreased to -110m below the present level, fluvial sediments from both the Red River and the Pearl River gradually increased in the slope regions of the northern SCS due to the coastline migrating forward to the outer continental shelf (Liu et al., 2010c, 2016b; Li et al., 2019; Cai et al., 2020). The lower values of ln(Ca/Ti) in the core XT-1 (Figure 3) also indicate an increase in terrigenous materials, resulting in a reduced presence of carbonate in the sediments due to dilution. As the studied area was closer to the estuary of the Red River, the enhanced terrigenous input to the vicinity of the studied core was likely derived mainly from the Red River through surface current during this period. This speculation is confirmed by the higher ln(Si/Al) values and mean particle size (Figure 3), suggesting a higher content of the coarser sediments and a closer provenance. Between 29.8 ka and ~23 ka, Taiwan (mean=44%) showed a slight decline in sediment contribution to the studied area (Figure 7), likely reflecting the dilution of Taiwan-sourced materials by the increased sediment supply from the Red River and the Pearl River.

Mean sediment fluxes from the four sediment sources in the studied area reach their maximum values almost simultaneously during the LGM (23 to 20.2 ka) (Figure 8), when sea level dropped to its lowest value of −120m (Grant et al., 2014). It has been reported that the DWC was strengthened during the LGM compared to the Holocene due to enhanced formation of North Pacific Deep Water (Zheng et al., 2016), which may have resulted in an enhanced sediment transport ability of the current. As sediments from southwestern Taiwan, the Pearl River and the EPR could be directly discharged to the outer continental

shelf and even the slope of the SCS during the LGM with sea level dropping, a strengthened DWC may consequently have increased the supply of sediments from these provenances to the studied area. The maximum flux of Red River-derived sediments during this period could be attributed to the exposure of continental shelf and the migration of the river mouth towards the edge of the outer continental shelf, resulting in a greater sediment supply to the studied area through the surface current. This explanation is consistent with the findings of Li et al., (2019), which reported a distinct increase in terrigenous input from the Red River in the western Xisha Trough during the LGM, leading to the development of turbidite sediments on the northwestern slope of the SCS. Sedimentation rates at the studied core also showed the highest mean values of 26.9 cm/ ka during this period (Figure 2), in accordance with the peak sedimentation rate of cores PC338, C7 and C120 in the slope regions of the western Xisha Trough (Li et al., 2019; Cai et al., 2020).

During the last deglaciation (20.2 to 13.5 ka), as the sea level rose to −60 m below its current level, the relative contribution (mean = 24%) and the MARs (mean = 2.1 g/cm^2/ka) of the Red River significantly decreased. This could be explained by the longer transport distance to the studied area, as the coastline retreated landward stepwise with rising sea level, which would have led to a substantial deposition of suspended particles on the continental shelf (Cai et al., 2020). In contrast, the relative contribution from the Pearl River (mean =14%) slightly increased with relatively high MARs values (mean = 1.5 g/cm^2/ka). This change is well correlated with the increased sediment flux from the Pearl River, characterized by a high content of kaolinite during the last deglaciation (18-14 ka) (Liu et al., 2010c, 2016a, 2017). Liu et al., (2017) proposed that the higher flux of the Pearl River-sourced sediment to the northern SCS during the last deglacial period was attributed to the combined effect of the continuous contribution of fluvial sediments from the Pearl River since the LGM, as well as the supply of reworked material derived from the Pearl River that was previously exposed on the shelf during the initial rise in sea level after 19 ka. Therefore, we suggest that the increased contribution of the Pearl River-originated sediment to the Xisha Trough during the last deglaciation was primarily caused by enhanced terrigenous input from the Pearl River. The relative contribution from Taiwan gradually increased during this stage, probably due to a reduction in the dilution effect caused by the decreased supply of sediment from the Red River. This explanation is supported by a decline in coarser sediments, as evidenced by lower values of ln(Si/Al), slit contents and mean grain size in the studied core (Figure 3), indicating a decreased contribution from proximal provenances.

There is no clear evidence of contributions from various sources in response to rapid climate change events during the last deglaciation (Figures 7 and 8), such as Heinrich and Melt Water Pulse events. This is likely related to the limited impact of rapid climate changes on the land-sea distribution caused by sea level fluctuations in the northern SCS. Analyses of digital elevation model and sediment thickness data have

indicated that the land-sea distribution and the paleo-coastline remained nearly unchanged in the northwestern SCS during the last deglacial period from 20 ka to 15 ka (Yao et al., 2009).

During the Holocene, as the sea-level continued to rise to its present level, Taiwan emerged as the predominant contributor of sediment in the studied area, accounting for a mean of 83% followed by the Red River at 16%, while the relative contribution from the Pearl River (mean = 1%) became negligible. The terrigenous input of core XT-1 experienced a significant decline during this period, as indicated by a noteworthy increase in the ln(Ca/Ti) values (Figure 3), suggesting a reduced dilution effect on carbonates. This change can be attributed to the greater distance between the main sediment sources and the studied area, which was caused by high sea levels (Siddall et al., 2003). The sediment during this stage was characterized by a higher mean clay content, lower ln(Si/Al) ratios, and smaller mean grain size (Figure 3), indicating a more distant provenance of sediments. Similar to the Red River, the fluvial sediments from the Pearl River were mainly deposited on the shelf as the coastline migrated landward (Liu et al., 2010c, 2016a, 2016b, 2017), resulting in minimal contribution to the studied area in the Xisha Trough.

Despite the generally low terrigenous input in the studied area during the Holocene, a distinct increase in the flux of Taiwan-sourced material (mean = 8.0 g/cm^2/ka) can be observed during the early to middle Holocene from ~12.0 ka to ~6.0 ka (Figure 8). This implies that the increased clay content in the studied core during this period (Figure 3) was primarily derived from Taiwan. The slightly weaker DWC during the Holocene compared to the LGM (Zheng et al., 2016) hampers the interpretation of the higher sediment contribution from Taiwan caused by the increased transport ability of the DWC. The geochemistry analysis of sediment core KNG5 (19°55.17′ N, 115°8.53′ E; water depth of 1085 m) in the northern SCS has revealed an increase in the terrigenous MARs from 12.0 ka to 5.5 ka, which was attributed to enhanced fluvial discharge from rivers in southwestern Taiwan due to intensified chemical weathering and physical erosion induced by the enhanced EASM (Huang et al., 2016). The increased discharge of Taiwan-derived materials may have also contributed to the carbonate-dilution event in the northern SCS, occurring during the early Holocene from 11.0 ka to 8.5 ka, which was attributed to the dominant terrigenous input of fine-grained detritus from Taiwan (Huang et al., 2015). In the studied core, the record of relatively low ln(Ca/Ti) values between 11.5 ka and 6.0 ka (Figure 3) is approximately in accordance with the increase in clay components from Taiwan during the early to middle Holocene. Therefore, the increase in relative contribution of Taiwanese sediment to the studied area in the Holocene may be caused by an enhanced input of clay material from Taiwan provenance resulting from the enhanced EASM.

Based on the aforementioned findings, we propose that on glacial-interglacial timescales, sea level fluctuations are the primary factor controlling changes in the provenances and their contributions to the northern slope of the Xisha Trough over the last 29.8 ka. Additionally, the enhanced deep-water current and EAM, respectively, had strong impacts on the contribution of Taiwanese sediments to the studied area

during the LGM and the early to middle Holocene periods. The limited responses of the different sources to rapid climate change during the last deglaciation can be attributed to the relatively stable land-sea distribution in the northwestern SCS.

5.3 Implications for the influence of the DWC on fine-grained sediments in the northern SCS and the Xisha Trough

In the northern SCS, Taiwan serves as the primary source of fine-grained terrigenous material during the late Quaternary, and its contribution varies across different parts of the northern SCS (Wan et al., 2010; Huang et al., 2016; Liu et al., 2010a, 2016a, 2016a, 2017). Clay mineral records in core XT-1 also indicate Taiwan is the primary sediment source for sediments on the northern slope of the Xisha Trough over that last 30 ka (Figure 6), with a gradual increase in its contribution, as evidenced by the illite+chrolite content (Figures 4 and 7). Interestingly, this changing pattern is generally consistent with the provenance change and contributions from Taiwanese sediments observed in cores MD05-2904 (19°27.40′ N, 116°16.37′ E, water depth of 2092 m) (Liu et al., 2010c), and GHE27L (115°20.81′ E, 19°50.85′ N, water depth of 1533 m) (Liu et al., 2016b), which are located at depths below 1,500m in the northern SCS. However, it differs significantly from the clay mineral records in cores GeoB16602-4 (18°57.12′N; 113°42.64′E; water depth of 970 m) and GeoB16601-6 (20°09.07′N; 116°14.38′E; water depth of 1012 m) from relatively shallower depths (above 1,500m) in the northern SCS (Liu et al., 2017), as well as cores PC 337 (17°15.0′ N, 110°06.0′ E, water depth of 516 m) and PC 338 (16°42.0′ N, 110°24.0′ E, water depth of 1,349 m) from the western Xisha Trough which are much closer in proximity (~200 km) to the studied area (Wan et al., 2015; Li et al., 2022).

The DWC is considered responsible for transporting fine-grained sediments, characterized by the high illite+chrolite content (mean=99%), southwestward from Taiwan along the lower slope regions in the northern SCS (Wan et al., 2010; Liu et al., 2016a). This current generally occurs at depth below 1,500m (Wang et al., 2011; Zhao et al., 2014) and, therefore, may exert a common influence on the sediment composition within its reach, probably resulting in consistent patterns in clay mineral records. This may explain the similar changing patterns of the illite+chrolite content and relative contribution from Taiwan provenance characterized by an overall increasing trend since the last glacial period in the core XT-1, as well as in cores MD05-2904 (Liu et al., 2010c) and GHE27L (Liu et al., 2016b). These similar changing patterns are likely caused by the dilution effect of fluvial sediments from the Red River and the Pearl River respectively, on the Taiwan-originated material. During the last glacial period of low sea level, the illite+chrolite content and the relative contribution from Taiwanese sediment in these cores was lower because of the increased sediment supplies from the Pearl River to the northern SCS, and from the Red River to the Xisha Trough. However, with sea level rising in the Holocene, the dilution effect on fine-grained sediments from Taiwan decreased due to the decline in both the Red River- and the Pearl River-sourced

sediments, which resulted in a higher illite+chrolite content in these cores and a greater relative contribution of sediments from Taiwan.

Although the EMA-driven surface current is also a potential dynamic for the southwestward transport of Taiwanese sediment and thus may impact the contribution of Taiwan provenance, it cannot account for the discrepancy of clay mineral records between cores from regions influenced by the DWC and those from shallower depths (above 1,000m) beyond the influence of the DWC in the northern SCS. The surface current primarily transports water masses and suspended particles in the upper water layer above ~350 m (Fang et al., 1998; Liu et al., 2016a). If this current is the primary transporting force of Taiwan-derived materials, sediment cores along its pathway should exhibit similar changing patterns in clay mineral records. However, cores GeoB16602-4 and GeoB16601-6, which were collected from the regions in the northern SCS with water depth less than 1000 m, show completely different patterns in the illite+chrolite content, compared to cores MD05-2904 and GHE27L below 1,500 m (Liu et al., 2017), making it difficult to attribute the discrepancy of clay mineral records to the surface current.

In the northwestern SCS, Sr-Nd isotope data of cores PC 337 and PC338 in the western Xisha Trough revealed that sediments mainly originated from the Red River since MIS 3 and were largely unaffected by Taiwan-derived materials (Wan et al., 2015; Li et al., 2022). However, in-situ observations by the sediment trap at station XS1 (17°24.5′ N, 110°55.0′E, water depth of 1,690m) indicated a DWC flowing from east to west in the northern part of the western Xisha Trough, along with a significant contribution of fine-grained detritus from Taiwan to the Xisha Trough (Liu et al., 2014a). Although little research has been conducted on the extent of the DWC in the entire Xisha Trough, the discrepancy in sediment source areas between core XT-1 in this study and cores from the southern part of the western Xisha Trough may suggest that the DWC flowing in the Xisha Trough does not reach the southern region of the western Xisha Trough, possibly due to its relatively shallow water depth. Previous simulations showed that after entering the Xisha Trough, the DWC flowed along the northern wall of the Xisha Trough to the west, affecting the sediment composition and deposition in the eastern and middle regions of the Xisha Trough (Chen et al., 2016). This could further explain the consistent patterns between the illite+chrolite content in core XT-1 and those in regions influenced by DWC in the northern SCS. However, the southern part of the western Xisha Trough, which is closer to the paleo-estuary of the Red River, may lack the influence of the DWC, leading to a completely distinct sediment source and sedimentary environment compared to XT-1.

6 Conclusions

The gravity core XT-1, collected from the northern slope of the Xisha Trough, has been utilized for the analysis of clay mineralogy, grain size composition and specific XRF core scanning elements, to assess

changes in the sediment provenance and their primary influencing factors over the last ~30 ka. Based on the findings of the present study, the following conclusions can be drawn:

(1) Clay mineral assemblages in the sediment core XT-1 mainly consist of illite, chlorite and kaolinite. Illite is the dominant clay mineral, accounting for a mean of 80%, followed by chlorite and kaolinite, each with a mean content of 9%. Smectite is present as a minor component, with a mean content of 2%. The contents of illite and chlorite, kaolinite and smectite have positive correlations with an overall increasing trend, but the contents of kaolinite and smectite show a negative correlation with that of illite/chlorite. Mean grain size and ln(Si/Al) ratios of the sediments exhibit three-phase changes with a gradual decreasing trend, suggesting an overall increase in fine-grained sediment and contributions from a more distant sediment source since the last glacial.

(2) Both the Red River and Taiwan were the primary sources of fine-grained sediments in the lower continental slope of the Xisha Trough before 20.2 ka BP, when sea level dropped approximately −100 to −120 m below present levels. However, Taiwan gradually became the dominant source of fine-grained sediments in the studied area, followed by the Red River, with the transgression since the deglaciation. The contribution from the Pearl River-originated material reached its maximum between 20.2 and 13.5 ka, responding to the increased terrigenous input of the Pearl River to the northern SCS during the last deglaciation. On the glacial-interglacial timescale, sea level fluctuations are the primary factor controlling changes in the provenance and sedimentation in the studied area over the last 29.8 ka. Additionally, during the LGM (23 to 20.2 ka) and the early to middle Holocene periods (12 to 5.5 ka), the strengthened deep-water current and EASM respectively exerted strong impacts on the contribution of Taiwanese sediments to the studied area.

(3) The changing pattern of the Taiwan provenance in the studied core is approximately consistent with those in the northern SCS, while differing from those in the southern regions of the western Xisha Trough. This discrepancy is attributed to the common influence of the DWC on slope regions in the studied area and the northern SCS, whereas the southern part of the western Xisha Trough likely remains unaffected by the DWC.

Acknowledgments

The sediment core XT-1 used in this study was collected onboard of R/V “SHIYAN3” implementing the open research cruise NORC2021-07 supported by NSFC Shiptime Sharing Project. We would like to thank two anonymous reviewers for their meticulous work and constructive suggestions. This research was supported by National Natural Science Foundation of China (Grant Nos. 42076073, 41606046), Guangdong Basic and Applied Basic Research Foundation (Grant Nos. 2020A1515010499, 2022A1515010932), Science and Technology Projects in Guangzhou (SL2024A04J01208), and the CAS Scholarship.

Data availability

All data used in this study are included within the paper, and the original data are stored and accessible at the "Science Data Bank" (https://www.scidb.cn/s/i6BvIr), or can be made available upon request via email (zhangqiang210@scsio.ac.cn).

References

Bahr, A., Lamy, F., Arz, H., Kuhlmann, H., Wefer, G. (2005). Late glacial to Holocene climate and sedimentation history in the NW Black Sea. Marine Geology, 214(4), 309-322.

Biscaye, P. E. (1965). Mineralogy and sedimentation of recent deep-sea clay in the Atlantic Ocean and adjacent seas and oceans. Geological Society of America Bulletin, 76(7), 803-832.

Boulay, S., Colin, C., Trentesaux, A., Frank, N., Liu, Z. (2005). Sediment sources and East Asian monsoon intensity over the last 450 ky. Mineralogical and geochemical investigations on South China Sea sediments. Palaeogeography, Palaeoclimatology, Palaeoecology, 228(3-4), 260-277.

Boulay, S., Colin, C., Trentesaux, A., Clain, S., Liu, Z., & Lauer-Leredde, C. (2007). Sedimentary responses to the Pleistocene climatic variations recorded in the South China Sea. Quaternary Research, 68(1), 162-172.

Cai, G., Li, S., Zhao, L., Zhong, L., Chen, H. (2020). Clay minerals, Sr-Nd isotopes and provenance of sediments in the northwestern South China Sea. Journal of Asian Earth Sciences, 202, 104531.

Calvert, S. E., Pedersen, T. F., & Thunell, R. C. (1993). Geochemistry of the surface sediments of the Sulu and South China Seas. Marine Geology, 114(3-4), 207-231.

Chamley, H., 1989. Clay Sedimentology. Springer, New York (623 pp.).

Chen, C. T. A. (2005). Tracing tropical and intermediate waters from the South China Sea to the Okinawa Trough and beyond. Journal of Geophysical Research: Oceans, 110(C5). doi.org/10.1029/2004JC002494

Chen, H., Harff, J., Qiu, Y., Osadczuk, A., Zhang, J., Tomczak, M., ... & Li, L. (2016). Last glacial cycle and seismic stratigraphic sequences offshore Western Hainan Island, NW South China Sea. Geological Society, London, Special Publications, 429(1), 99-121.

Clift, P., Lee, J. I., Clark, M. K., Blusztajn, J. (2002). Erosional response of South China to arc rifting and monsoonal strengthening; a record from the South China Sea. Marine Geology, 184(3-4), 207-226.

Clift, P. D., Long, H. V., Hinton, R., Ellam, R. M., Hannigan, R., Tan, M. T., ... Duc, N. A. (2008). Evolving east Asian river systems reconstructed by trace element and Pb and Nd isotope variations in modern and ancient Red River-Song Hong sediments. Geochemistry, Geophysics, Geosystems, 9(4). doi.org/10.1029/2007GC001867

Clift, P. D., Wan, S., Blusztajn, J. (2014). Reconstructing chemical weathering, physical erosion and monsoon intensity since 25 Ma in the northern South China Sea: a review of competing proxies. Earth-Science Reviews, 130, 86-102

Cao, L., Liu, J., Shi, X., He, W., & Chen, Z. (2019). Source-to-sink processes of fluvial sediments in the northern South China Sea: constraints from river sediments in the coastal region of South China. Journal of Asian Earth Sciences, 185, 104020. doi.org/10.1016/j.jseaes.2019.104020

Clemens, S. C., Holbourn, A., Kubota, Y., Lee, K. E., Liu, Z., Chen, G., et al. (2018). Precession-band variance missing from East Asian monsoon runoff. Nature communications, 9(1), 3364. doi.org/10.1038/s41467-018-05814-0

Dadson, S. J., Hovius, N., Chen, H., Dade, W. B., Hsieh, M. L., Willett, S. D., ... Lin, J. C. (2003). Links between erosion, runoff variability and seismicity in the Taiwan orogen. Nature, 426(6967), 648-651.

Dai, L., Weng, C., Mao, L. (2015). Patterns of vegetation and climate change in the northern South China Sea during the last glaciation inferred from marine palynological records. Palaeogeography, Palaeoclimatology, Palaeoecology, 440, 249-258.

Ehrmann, W. (1998). Implications of late Eocene to early Miocene clay mineral assemblages in McMurdo Sound (Ross Sea, Antarctica) on paleoclimate and ice dynamics. Palaeogeography, Palaeoclimatology, Palaeoecology, 139(3-4), 213-231.

Fang, G.H., Fang,W.D., Fang, Y.,Wang, K., 1998. A survey of studies on the South China Sea upper ocean circulation. Acta Oceanogr. Taiwan. 37 (1), 1–16.

Fang, G., Wang, G., Fang, Y., Fang, W. (2012). A review on the South China Sea western boundary current. Acta Oceanologica Sinica, 31, 1-10.

Ge, Q., Xue, G. Z., Ye, L., Xu, D., Zhao, J., Chu, F. (2019). The spatial distribution of major and trace elements of surface sediments in the northeastern Beibu Gulf of the South China Sea. Acta Oceanologica Sinica, 38, 93-102.

Gingele, F. X. (1996). Holocene climatic optimum in Southwest Africa—evidence from the marine clay mineral record. Palaeogeography, Palaeoclimatology, Palaeoecology, 122(1-4), 77-87.

Grant, K. M., Rohling, E. J., Ramsey, C. B., Cheng, H., Edwards, R. L., Florindo, F., ... & Williams, F. (2014). Sea-level variability over five glacial cycles. Nature communications, 5(1), 5076. doi: 10.1038/ncomms6076

Guo, Z., Biscaye, P., Wei, L., Chen, X., Peng, S., Liu, T. (2000). Summer monsoon variations over the last 1.2 Ma from the weathering of loess-soil sequences in China. Geophysical Research Letters, 27(12), 1751-1754.

Hanebuth, T., Stattegger, K., Grootes, P. M. (2000). Rapid flooding of the Sunda Shelf: a late-glacial sea-level record. Science, 288(5468), 1033-1035.

He, L.S., Wang, G.Y., Shi, X.C., 1980. Xisha Trough-a Cenozoic rift. Geol. Rev. 26 (6), 486 – 489 (in Chinese).

Hu, B., Li, J., Cui, R., Wei, H., Zhao, J., Li, G., Bai, F. (2014). Clay mineralogy of the riverine sediments of Hainan Island, South China Sea: Implications for weathering and provenance. Journal of Asian Earth Sciences, 96, 84-92.

Huang, E., Tian, J., Qiao, P., Wan, S., Xie, X., & Yang, W. (2015). Early interglacial carbonate-dilution events in the South China Sea: Implications for strengthened typhoon activities over subtropical East Asia. Quaternary Science Reviews, 125, 61-77.

Huang, J., Wan, S., Xiong, Z., Zhao, D., Liu, X., Li, A., & Li, T. (2016). Geochemical records of Taiwan-sourced sediments in the South China Sea linked to Holocene climate changes. Palaeogeography, Palaeoclimatology, Palaeoecology, 441, 871-881.

Kuhnt, W., Holbourn, A., Xu, J., Opdyke, B., De Deckker, P., Röhl, U., Mudelsee, M. (2015). Southern Hemisphere control on Australian monsoon variability during the late deglaciation and Holocene. Nature Communications, 6, 5916. doi.org/10.1038/ ncomms6916

Lei, C., Alves, T. M., Ren, J., Tong, C. (2020). Rift structure and sediment infill of hyperextended continental crust: insights from 3D seismic and well data (Xisha Trough, South China Sea). Journal of Geophysical Research: Solid Earth, 125(5), e2019JB018610. doi.org/10.1029/2019JB018610

Li, G., Yan, W., Zhong, L., Xia, Z., & Wang, S. (2015). Provenance of heavy mineral deposits on the northwestern shelf of the South China Sea, evidence from single-mineral chemistry. Marine Geology, 363, 112-124.

Li, M., Ouyang, T., Tian, C., Zhu, Z., Peng, S., Tang, Z., ... & Peng, X. (2019). Sedimentary responses to the East Asian monsoon and sea level variations recorded in the northern South China Sea over the past 36 kyr. Journal of Asian Earth Sciences, 171, 213-224.

Li, M., Ouyang, T., Zhu, Z., Tian, C., Peng, S., Zhong, H., ... & Qiu, Y. (2022). Reconstruction of chemical weathering Intensity and Asian Summer Monsoon Evolution in the Red River Basin over the past 36 kyr. Paleoceanography and Paleoclimatology, 37(5), e2021PA004397. doi.org/10.1029/2021PA004397

Liu, F., Wu, L. (2006). Topographic and morphologic characteristics and genesis analysis of Xisha Trough sea area in the South China Sea. Marine Geology and Quaternary Geology, 26(3), 7-14. (in Chinese with English abstract)

Liu, J., Xiang, R., Chen, M., Chen, Z., Yan, W., & Liu, F. (2011). Influence of the Kuroshio current intrusion on depositional environment in the Northern South China Sea: Evidence from surface sediment records. Marine Geology, 285(1-4), 59-68.

Liu, J., Xiang, R., Chen, Z., Chen, M., Yan, W., Zhang, L., Chen, H. (2013). Sources, transport and deposition of surface sediments from the South China Sea. Deep Sea Research Part I: Oceanographic Research Papers, 71, 92-102.

Liu, J., Clift, P. D., Yan, W., Chen, Z., Chen, H., Xiang, R., Wang, D. (2014a). Modern transport and deposition of settling particles in the northern South China Sea: Sediment trap evidence adjacent to Xisha Trough. Deep Sea Research Part I: Oceanographic Research Papers, 93, 145-155.

Liu, Y., Gao, S., Wang, Y. P., Yang, Y., Long, J., Zhang, Y., & Wu, X. (2014b). Distal mud deposits associated with the Pearl River over the northwestern continental shelf of the South China Sea. Marine Geology, 347, 43-57.

Liu, J., Steinke, S., Vogt, C., Mohtadi, M., De Pol-Holz, R., & Hebbeln, D. (2017). Temporal and spatial patterns of sediment deposition in the northern South China Sea over the last 50,000 years. Palaeogeography, Palaeoclimatology, Palaeoecology, 465, 212-224.

Liu, J. P., Xue, Z., Ross, K., Wang, H. J., Yang, Z. S., Li, A. C., Gao, S. (2009). Fate of Sediments Delivered to the Sea by Asian Large Rivers. The Sedimentary Record, 7(4), 4-9.

Liu, Z., Trentesaux, A., Clemens, S. C., Colin, C., Wang, P., Huang, B., Boulay, S. (2003a). Clay mineral assemblages in the northern South China Sea: implications for East Asian monsoon evolution over the past 2 million years. Marine Geology, 201(1-3), 133-146.

Liu, Z., Alain, T., Clemens, S. C., Wang, P. (2003b). Quaternary clay mineralogy in the northern South China Sea (ODP Site 1146) Implications for oceanic current transport and East Asian monsoon evolution. Science in China Series D: Earth Sciences, 46, 1223-1235.

Liu, Z., Colin, C., Huang, W., Le, K. P., Tong, S., Chen, Z., & Trentesaux, A. (2007a). Climatic and tectonic controls on weathering in south China and Indochina Peninsula: Clay mineralogical and geochemical investigations from the Pearl, Red, and Mekong drainage basins. Geochemistry, Geophysics, Geosystems, 8(5). doi.org/10.1029/2006GC001490

Liu, Z., Colin, C., Huang, W., Chen, Z., Trentesaux, A., Chen, J. (2007b). Clay minerals in surface sediments of the Pearl River drainage basin and their contribution to the South China Sea. Chinese Science Bulletin, 52(8), 1101-1111.

Liu, Z., Zhao, Y., Li, J., & Colin, C. (2007c). Late Quaternary clay minerals off Middle Vietnam in the western South China Sea: Implications for source analysis and East Asian monsoon evolution. Science in China Series D: Earth Sciences, 50(11), 1674-1684.

Liu, Z.F., Tuo,S.T., Colin,C., Liu,J.T., Huang,C.Y., Selvaraj, K., Chen,C.T.A., Zhao,Y.L., Siringan, F.P., Boulay,S., Chen,Z., (2008). Detrital fine-grained sediment contribution from Taiwan to the northern South China Sea and its relation to regional oceancirculation. Mar.Geol255, 149–155.

Liu, Z., Zhao, Y., Colin, C., Siringan, F. P., Wu, Q. (2009). Chemical weathering in Luzon, Philippines from clay mineralogy and major-element geochemistry of river sediments. Applied Geochemistry, 24(11), 2195-2205.

Liu, Z., Colin, C., Li, X., Zhao, Y., Tuo, S., Chen, Z., ... Huang, K. F. (2010a). Clay mineral distribution in surface sediments of the northeastern South China Sea and surrounding fluvial drainage basins: Source and transport. Marine Geology, 277(1-4), 48-60.

Liu, J., Chen, M., Chen, Z., Yan, W. (2010b). Clay mineral distribution in surface sediments of the South China Sea and its significance for in sediment sources and transport. Chinese Journal of Oceanology and Limnology, 28(2), 407-415.

Liu, Z., Li, X., Colin, C., Ge, H. (2010c). A high-resolution clay mineralogical record in the northern South China Sea since the Last Glacial Maximum, and its time series provenance analysis. Chinese Science Bulletin, 55, 4058-4068.

Liu, Z., Wang, H., Hantoro, W. S., Sathiamurthy, E., Colin, C., Zhao, Y., Li, J. (2012a). Climatic and tectonic controls on chemical weathering in tropical Southeast Asia (Malay Peninsula, Borneo, and Sumatra). Chemical Geology, 291, 1-12.

Liu, J., Yan, W., Chen, Z., Lu, J. (2012b). Sediment sources and their contribution along northern coast of the South China Sea: Evidence from clay minerals of surface sediments. Continental Shelf Research, 47, 156-164.

Liu, Z., Zhao, Y., Colin, C., Stattegger, K., Wiesner, M. G., Huh, C. A., ... Li, Y. (2016a). Source-to-sink transport processes of fluvial sediments in the South China Sea. Earth-Science Reviews, 153, 238-273.

Liu, J., Xiang, R., Kao, S. J., Fu, S., & Zhou, L. (2016b). Sedimentary responses to sea-level rise and Kuroshio Current intrusion since the Last Glacial Maximum: Grain size and clay mineral evidence from the northern South China Sea slope. Palaeogeography, Palaeoclimatology, Palaeoecology, 450, 111-121.

Lyu, A. Q., Yin, Q. Z., Crucifix, M., Sun, Y. B. (2021). Diverse regional sensitivity of summer precipitation in East Asia to ice volume, CO2 and astronomical forcing. Geophysical Research Letters, 48(7), e2020GL092005. doi.org/10.1029/2020GL092005

Meckler, A. N., Sigman, D. M., Gibson, K. A., François, R., Martínez-García, A., Jaccard, S. L., et al. (2013). Deglacial pulses of deep ocean silicate into the subtropical North Atlantic Ocean. Nature, 495(7442), 495–498. doi.org/10.1038/nature12006

Milliman, J. D., Syvitski, J. P. (1992). Geomorphic/tectonic control of sediment discharge to the ocean: the importance of small mountainous rivers. The journal of Geology, 100(5), 525-544.

Milliman, J.D., Farnsworth, K.L., 2011. River Discharge to the Coastal Ocean: A Global Synthesis. Cambridge University Press, Cambridge (384 pp.)

Nan, F., Xue, H., Yu, F. (2015). Kuroshio intrusion into the South China Sea: A review. Progress in Oceanography, 137, 314-333.

Osipov, V.I. 2012. Density of clay minerals. Soil Mechanics and Foundation Engineering. 48 (6), 231–240

Qu, T., Girton, J. B., Whitehead, J. A. (2006). Deepwater overflow through Luzon strait. Journal of Geophysical Research: Oceans, 111(C1). doi.org/10.1029/2005JC003139

Petschick, R., Kuhn, G., Gingele, F. (1996). Clay mineral distribution in surface sediments of the South Atlantic: sources, transport, and relation to oceanography. Marine Geology, 130(3-4), 203-229.

Rasmussen, S. O., Andersen, K. K., Svensson, A. M., Steffensen, J. P., Vinther, B. M., Clausen, H. B., ... & Ruth, U. (2006). A new Greenland ice core chronology for the last glacial termination. Journal of Geophysical Research: Atmospheres, 111(D6). doi.org/10.1029/2005JD006079

Shao, L., Li, X., Geng, J., Pang, X., Lei, Y., Qiao, P., ... Wang, H. (2007). Deep water bottom current deposition in the northern South China Sea. Science in China Series D: Earth Sciences, 50(7), 1060-1066.

Shao, L., Qiao, P., Pang, X., Wei, G., Li, Q., Miao, W., Li, A. (2009). Nd isotopic variations and its implications in the recent sediments from the northern South China Sea. Chinese Science Bulletin, 54(2), 311-317.

Shaw, P. T., Chao, S. Y. (1994). Surface circulation in the South China sea. Deep Sea Research Part I: Oceanographic Research Papers, 41(11-12), 1663-1683.

Siddall, M., Rohling, E. J., Almogi-Labin, A., Hemleben, C., Meischner, D., Schmelzer, I., & Smeed, D. A. (2003). Sea-level fluctuations during the last glacial cycle. Nature, 423(6942), 853-858.

Southon, J., Kashgarian, M., Fontugne, M., Metivier, B., & Yim, W. W. (2002). Marine reservoir corrections for the Indian Ocean and Southeast Asia. Radiocarbon, 44(1), 167-180.

Steinke, S., Kienast, M., & Hanebuth, T. (2003). On the significance of sea-level variations and shelf paleo-morphology in governing sedimentation in the southern South China Sea during the last deglaciation. Marine Geology, 201(1-3), 179-206.

Steinke, S., Hanebuth, T. J., Vogt, C., Stattegger, K. (2008). Sea level induced variations in clay mineral composition in the southwestern South China Sea over the past 17,000 yr. Marine Geology, 250(3-4), 199-210.

Tanabe, S., Hori, K., Saito, Y., Haruyama, S., Kitamura, A. (2003). Song Hong (Red River) delta evolution related to millennium-scale Holocene sea-level changes. Quaternary Science Reviews, 22(21-22), 2345-2361.

Tanabe, S., Saito, Y., Vu, Q. L., Hanebuth, T. J., Ngo, Q. L., Kitamura, A. (2006). Holocene evolution of the Song Hong (Red River) delta system, northern Vietnam. Sedimentary Geology, 187(1-2), 29-61.

Tian, X., Xu, F. J., Wu, S. Z., Zhang, J., Guo, C., Dong, J. (2015). Clay mineral characteristics and provenance of continental shelf sediments in eastern Hainan Island since middle Holocene. Earth Science-Journal of China University of Geosciences, 40(9), 1497-1504. Doi: 10.3799/dqkx.2015.134 (in Chinese with English abstract)

Wan, S., Li, A., Clift, P. D., Stuut, J. B. W. (2007). Development of the East Asian monsoon: mineralogical and sedimentologic records in the northern South China Sea since 20 Ma. Palaeogeography, Palaeoclimatology, Palaeoecology, 254(3-4), 561-582.

Wan, S., Li, A., Xue, K. H, Yin, X. M. (2008). Characteristics of clay minerals in the northern South China Sea and its implications for evolution of East Asian Monsoon since Miocene. Journal of China University of Geosciences, 19(1), 23-37.

Wan, S., Li, A., Clift, P. D., Wu, S., Xu, K., Li, T. (2010). Increased contribution of terrigenous supply from Taiwan to the northern South China Sea since 3 Ma. Marine Geology, 278(1-4), 115-121.

Wan, S., Toucanne, S., Clift, P. D., Zhao, D., Bayon, G., Yu, Z., ... Li, T. (2015). Human impact overwhelms long-term climate control of weathering and erosion in southwest China. Geology, 43(5), 439-442.

Wang, Y., Cheng, H., Edwards, R. L., Kong, X., Shao, X., Chen, S., ... An, Z. (2008). Millennial-and orbital-scale changes in the East Asian monsoon over the past 224,000 years. Nature, 451(7182), 1090-1093.

Wang, A., Du, Y., Peng, S., Liu, K., Huang, R. X. (2018). Deep water characteristics and circulation in the South China Sea. Deep Sea Research Part I: Oceanographic Research Papers, 134, 55-63.

Wang, G., Xie, S. P., Qu, T., Huang, R. X. (2011). Deep South China Sea circulation. Geophysical Research Letters, 38(5). doi.org/10.1029/2010GL046626

Wang, L., Sarnthein, M., Erlenkeuser, H., Grimalt, J., Grootes, P., Heilig, S., Pflaumann, U. (1999). East Asian monsoon climate during the Late Pleistocene: high-resolution sediment records from the South China Sea. Marine Geology, 156(1-4), 245-284

Wang, P., Wang, L., Bian, Y., Jian, Z. (1995). Late Quaternary paleoceanography of the South China Sea: surface circulation and carbonate cycles. Marine Geology, 127(1-4), 145-165.

Wang, P., Li, Q., 2009. Oceanographical and geological background. In: Wang, P., Li, Q. (Eds.), The South China Sea. Springer, Netherlands, pp. 25–73.

Wei, G., Liu, Y., Ma, J., Xie, L., Chen, J., Deng, W., Tang, S. (2012). Nd, Sr isotopes and elemental geochemistry of surface sediments from the South China Sea: implications for provenance tracing. Marine Geology, 319, 21-34.

Xiang, R., Chen, M., Li, Q., Liu, J., Zhang, L., & Lu, J. (2009). Planktonic foraminiferal records of East Asia monsoon changes in the southern South China Sea during the last 40,000 years. Marine Micropaleontology, 73(1-2), 1-13.

Xue, H., Chai, F., Pettigrew, N., Xu, D., Shi, M., & Xu, J. (2004). Kuroshio intrusion and the circulation in the South China Sea. Journal of Geophysical Research: Oceans, 109(C2). doi.org/10.1029/2002JC001724

Yao, Y., Harff, J., Meyer, M., & Zhan, W. (2009). Reconstruction of paleocoastlines for the northwestern South China Sea since the Last Glacial Maximum. Science in China Series D: Earth Sciences, 52(8), 1127-1136.

Yu, Z., Colin, C., Wan, S., Saraswat, R., Song, L., Xu, Z., ... Kumar, A. (2019). Sea level-controlled sediment transport to the eastern Arabian Sea over the past 600 kyr: Clay minerals and SrNd isotopic evidence from IODP Site U1457. Quaternary Science Reviews, 205, 22-34.

Yu, Z., Colin, C., Bassinot, F., Wan, S., Bayon, G. (2020). Climate-driven weathering shifts between highlands and floodplains. Geochemistry, Geophysics, Geosystems, 21(7), e2020GC008936.

Zhang, J., Wang, D.R., Jennerjahn, T., Dsikowitzky, L., 2013. Land–sea interactions at the east coast of Hainan Island, South China Sea: a synthesis. Cont. Shelf Res. 57, 132–142.

Zhang, Q., Chen, M., Liu, J., Yu, Z., Zhang, L., Xiang, R. (2015). Clay mineral assemblages at IODP Site U1340 in the Bering Sea and their paleoclimatic significance. Science China Earth Sciences, 58, 707-717.

Zhang, W., Wei, X., Jinhai, Z., Yuliang, Z., & Zhang, Y. (2012). Estimating suspended sediment loads in the Pearl River Delta region using sediment rating curves. Continental Shelf Research, 38, 35-46.

Zhao, D., Wan, S., Lu, Z., Zhai, L., Feng, X., Shi, X., Li, A. (2020). Response of heterogeneous rainfall variability in East Asia to Hadley circulation reorganization during the late Quaternary. Quaternary Science Reviews, 247, 106562. doi.org/10.1016/j.quascirev.2020.106562

Zhao, W., Zhou, C., Tian, J., Yang, Q., Wang, B., Xie, L., & Qu, T. (2014). Deep water circulation in the Luzon Strait. Journal of Geophysical Research: Oceans, 119(2), 790-804. doi.org/10.1002/2013JC009587

Zheng, X., Kao, S., Chen, Z., Menviel, L., Chen, H., Du, Y., ... Zhang, X. U. (2016). Deepwater circulation variation in the South China Sea since the last glacial maximum. Geophysical Research Letters, 43(16), 8590-8599.

Zhong, G., Peng, X. (2021). Transport and accumulation of plastic litter in submarine canyons—The role of gravity flows. Geology, 49(5), 581-586.

Zhu, Y., Sun, J., Wang, Y., Li, S., Xu, T., Wei, Z., Qu, T. (2019). Overview of the multi-layer circulation in the South China Sea. Progress in Oceanography, 175, 171-182.

Figures and table captions

Table 1 The AMS ^{14}C dating ages and calibrated calendar ages for plankton foraminifera from core XT-1.

Sample depth (cm)	Plankton foraminefera species	^{14}C age (a BP)	2σ cal. age range[1]	Cal. median age (a BP)
17	*G. ruber*	2050±30	1434-1797	1618
46	*G. ruber*	5730±30	5925-6267	6098
87	*G. ruber*	8910 ± 30	9416-9787	9580
121	*G. ruber*	10270 ± 30	11698-12237	11943
146	*G. ruber*	13480±50	15318-15872	15598
195	*G. ruber + G. saccculifer*	16870 ±50	19376-19917	19643
230	*G. ruber + G. saccculifer*	17950 ±60	20645-21261	20934
275	*G. ruber + G. saccculifer*	19370 ±50	22372-22874	22615
315	*G. ruber + G. saccculifer*	22840 ±80	26002-26724	26329
342	*G. ruber*	26060±130	29213-29919	29595

[1]2σ enclosing 95.4% of probability distribution.

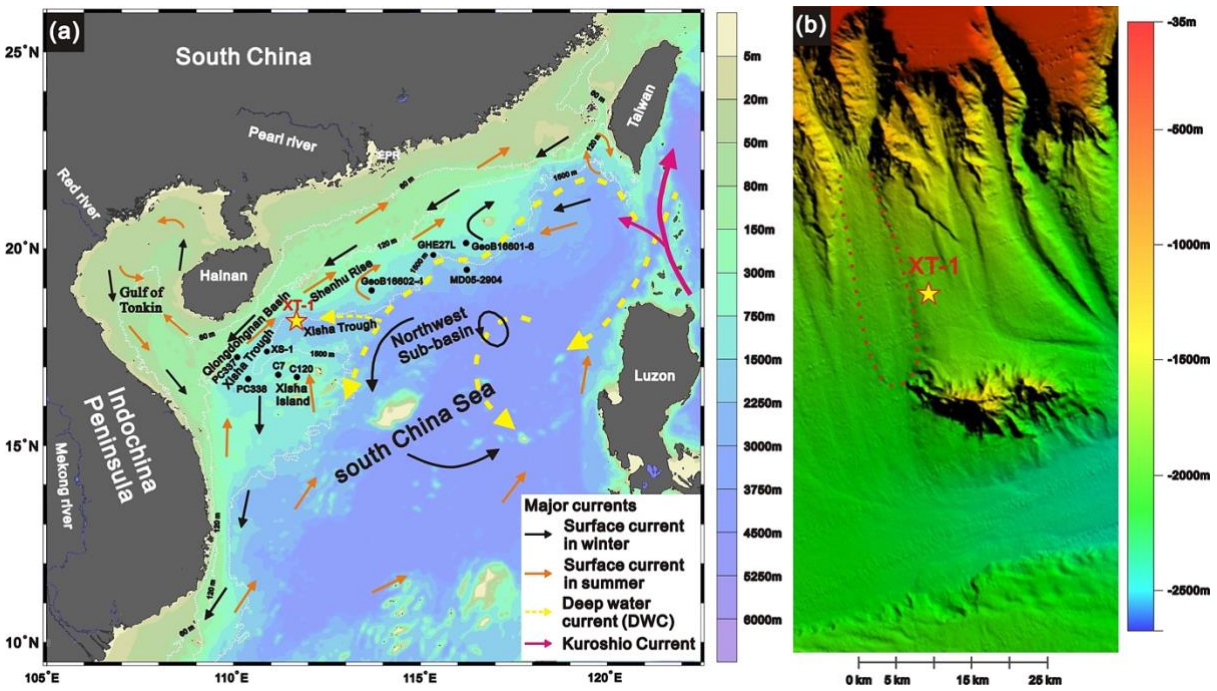

Figure 1 (a) The location of gravity core XT-1 (the star pentagon) and circulation patterns in the SCS. (b) the bathymetric map for the vicinity of the core XT-1, which indicates the core is situated on the bank of the submarine canyon (the area enclosed by the red dashed line). The locations of sediment trap and cores (black dots) discussed in the study are also shown, including XS1 (Liu et al., 2014a), PC337 (Wan et al., 2015), PC338 (Li et al., 2019, 2022), C7 and C120 (Cai et al., 2020), GHE27L (Liu et al., 2016b) and M05-2904 (Liu et al., 2010c). The circulation patterns in the SCS is modified after Liu et al. (2016a), with the DWC in the Xisha Trough deduced after Qu et al., (2006), Liu et al., (2014a) and Chen et al., (2016). The white dashed lines represent −60 m, −120 m, and 1,500 isobaths, respectively.

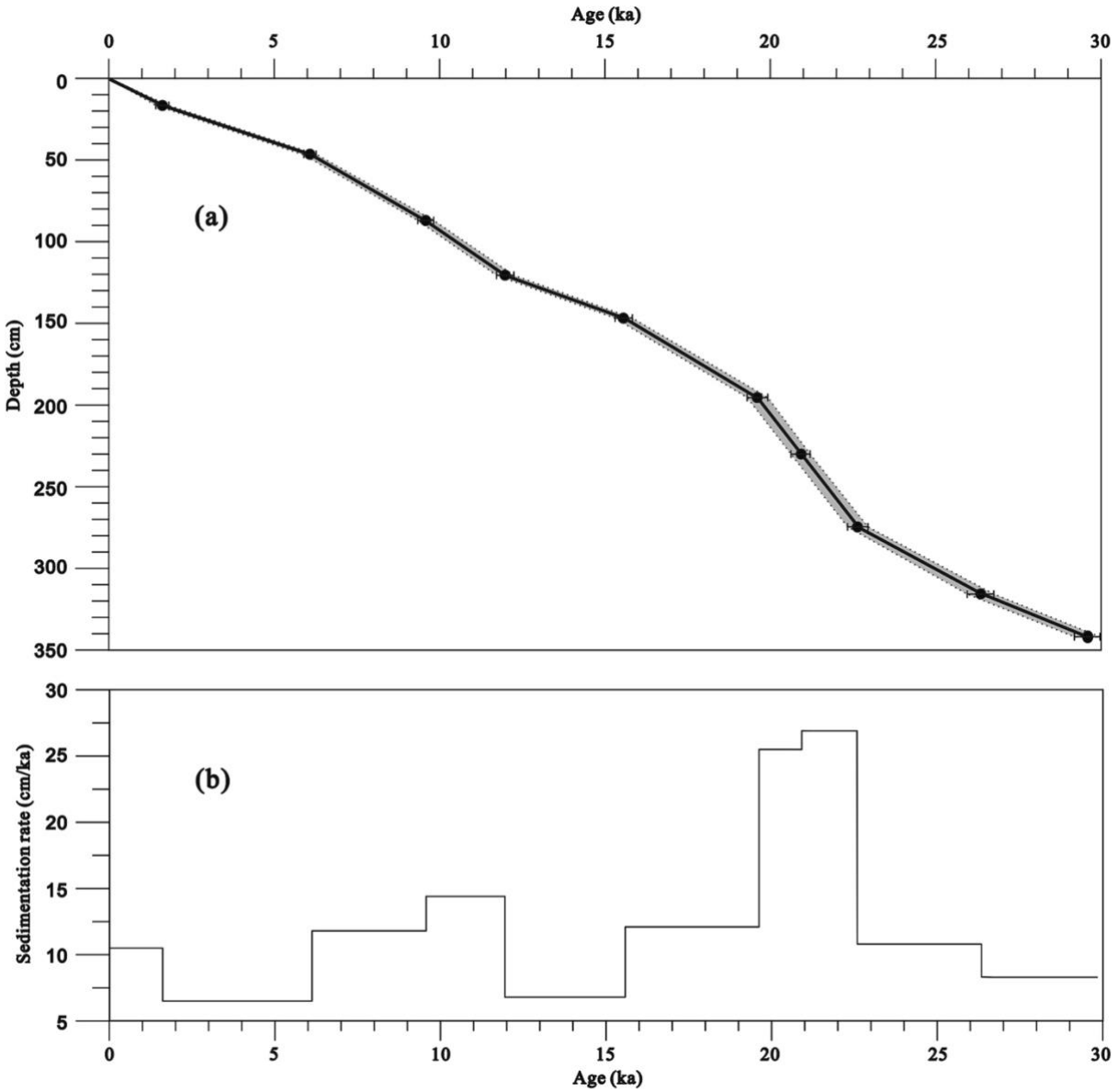

Figure 2 Age model (a) and linear sedimentation rate (b) of core XT-1 based on the calibrated AMS ^{14}C dates. Black dots in represent the median ages of the calibrated AMS ^{14}C dates; the horizontal error bars indicate the 2σ calibrated age range; the black solid line shows the optimal age model; the gray area between black dashed lines denote chronological uncertainties (95% probability interval).

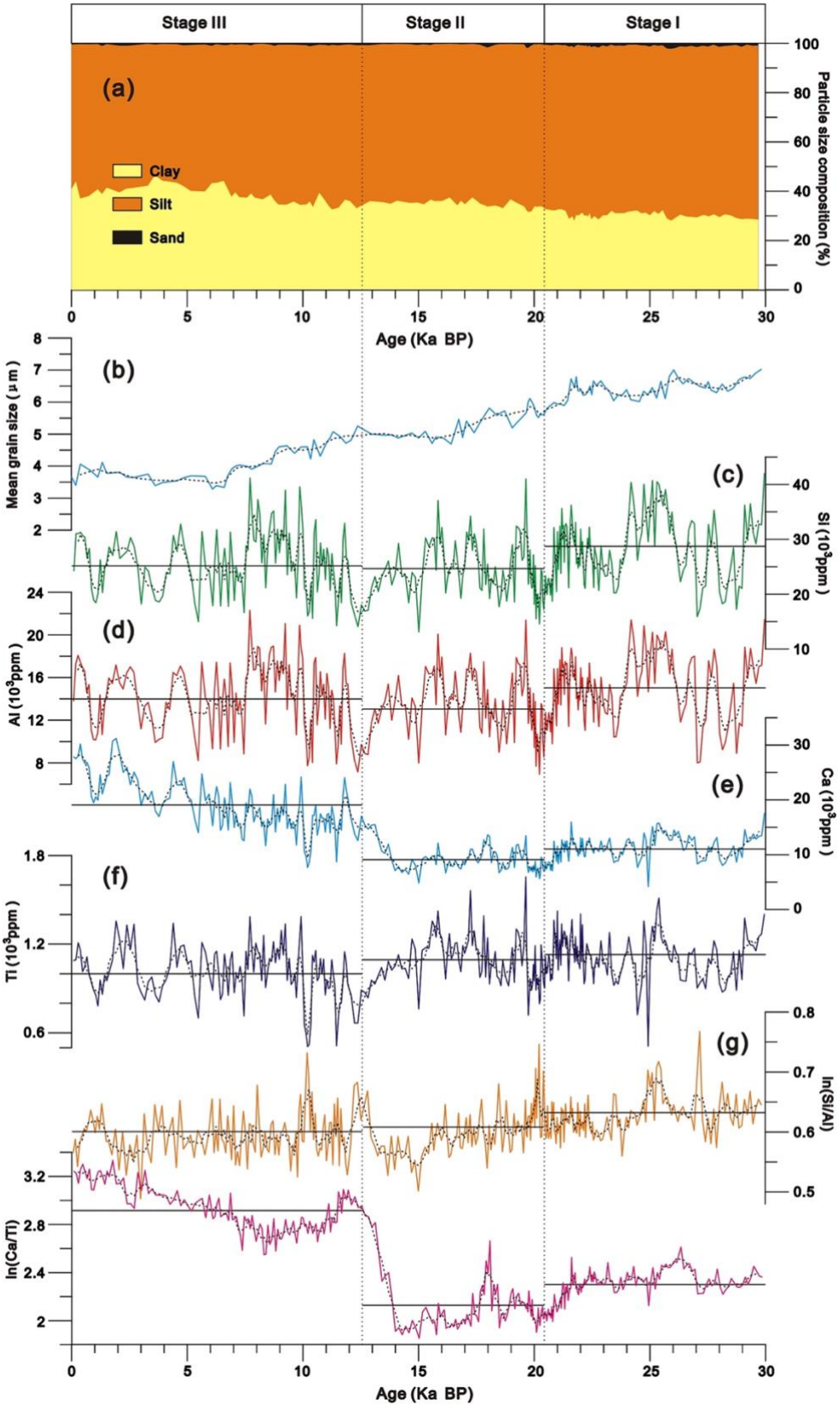

Figure 3 Downcore profiles of: (a) percentages of different particle size components, (b) the mean grain size, the concentrations of elements (c) Si, (d) Al, (e) Ca, (f) Ti, and the ln-ratios of (g) Si/Al, (h) Ca/Ti. The dashed black curved lines in Figures 3b–3h indicate running average values; the horizontal solid black lines

Figures 3c–3h represent the mean values during various periods; the vertical black dashed lines denote the boundaries of each stage.

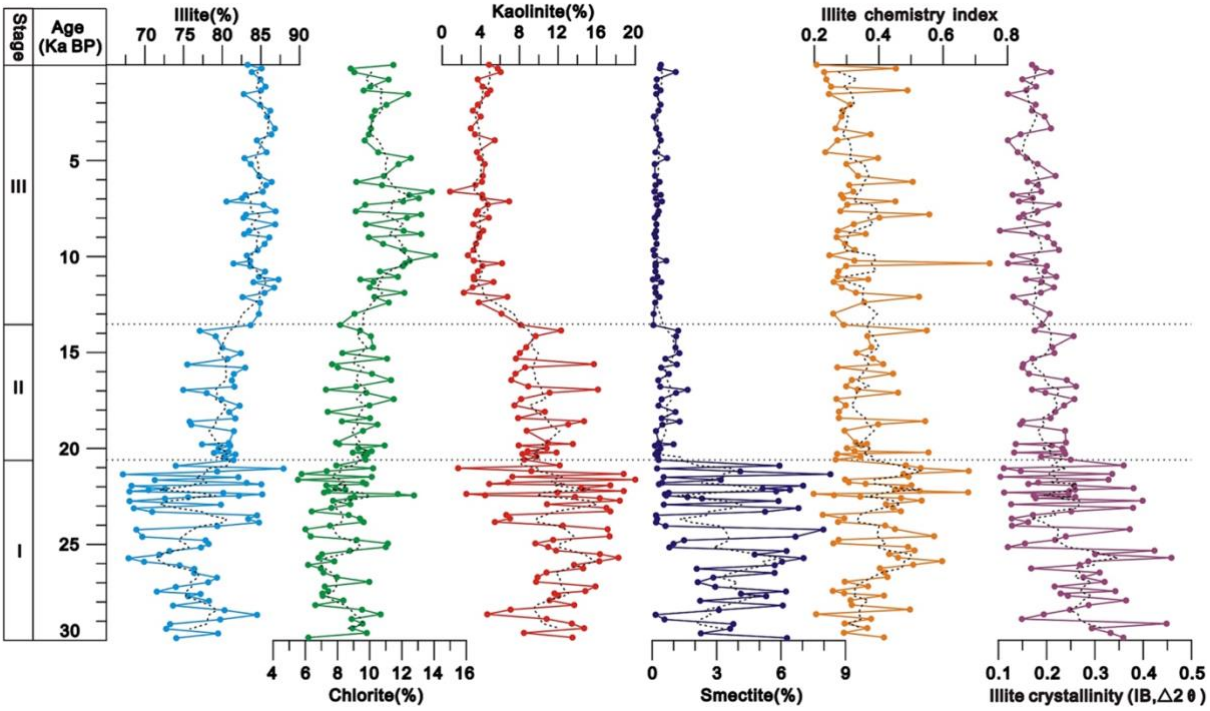

Figure 4 The contents of smectite, illite, kaolinite, and chlorite, as well as illite chemistry index and illite crystallinity in the sediment core XT-1. The dashed black curved lines present running average values; the horizontal dashed lines indicate the boundary of each stage.

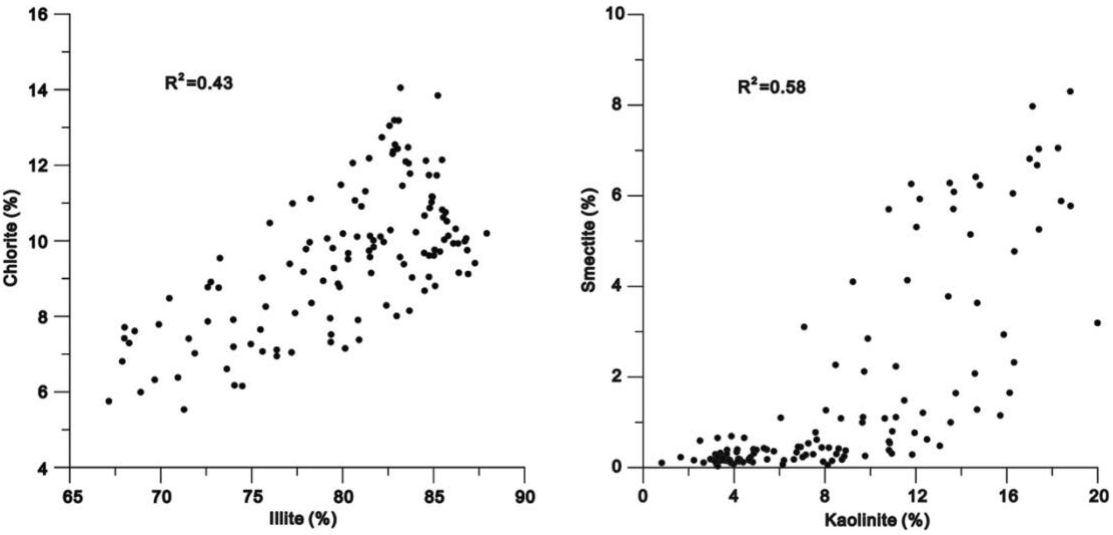

Figure 5 Correlations between clay minerals in sediments from core XT-1.

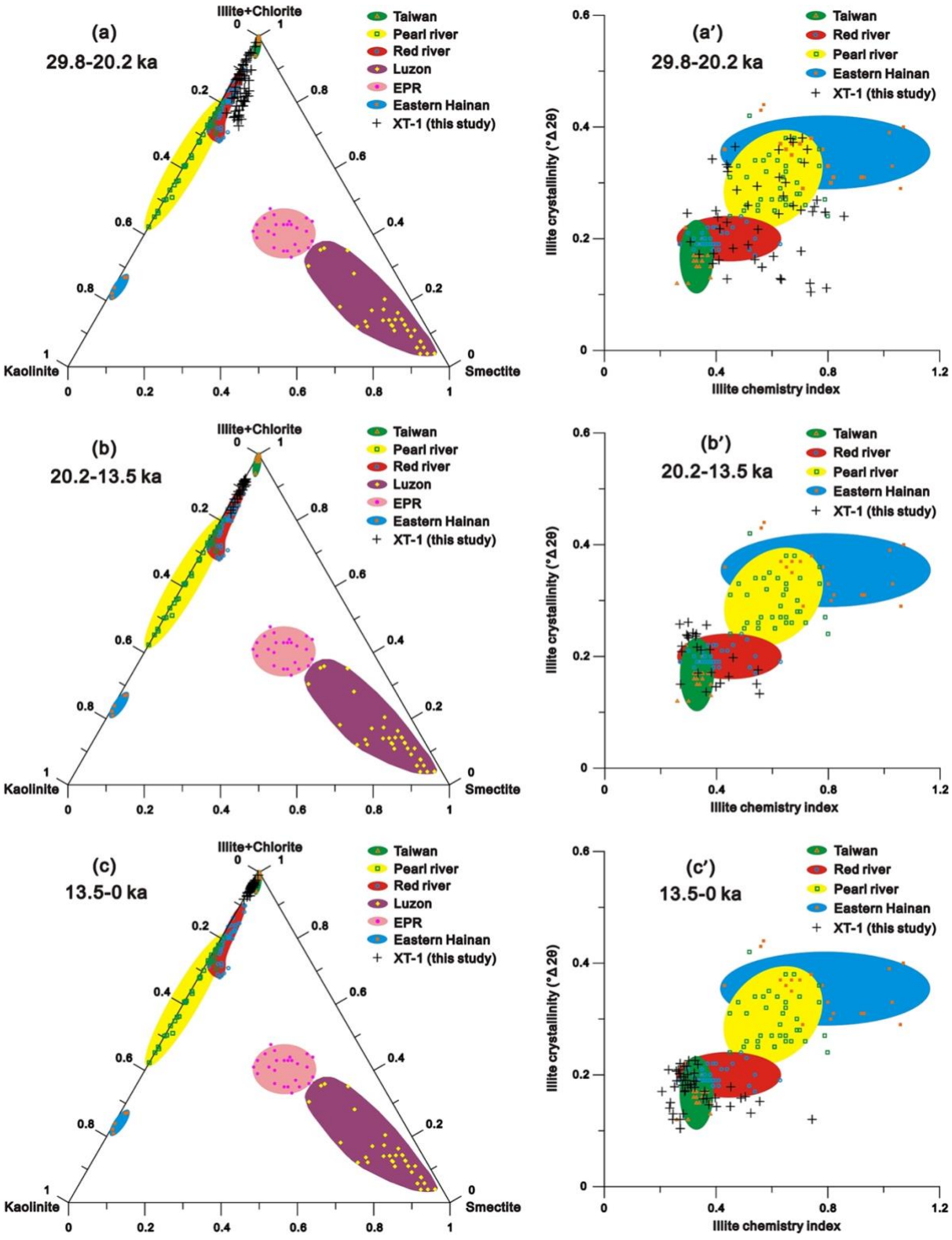

Figure 6 Ternary diagrams of clay mineral assemblages for sediments in core XT-1 (black crosses) during the periods: (a) 29.8-20.2 ka, (b) 20.2–13.5 ka, and (c) 13.5–0 ka compared with those from modern river sediments of Red River (recalculated from Liu et al., 2007a), Taiwan (recalculated from Liu et al., 2007b, 2008), the Pearl River (recalculated from Liu et al., 2007a), the area east of the Pearl River (Liu et al., 2016b), Hainan (Hu et al., 2014, recalculated from Liu et al., 2016a), and Luzon (recalculated from Liu et al., 2010a); the comparison of the illite crystallinity and the illite chemistry index in sediments from the studied core during the periods (a′) 29.8-20.2 ka, (b′) 20.2–13.5 ka, and (c′) 13.5–0 ka with those of modern river

sediments from the Red River (Liu et al., 2007a), Taiwan (Liu et al., 2008), the Pearl River (Liu et al., 2007a) and Hainan (Hu et al., 2014).

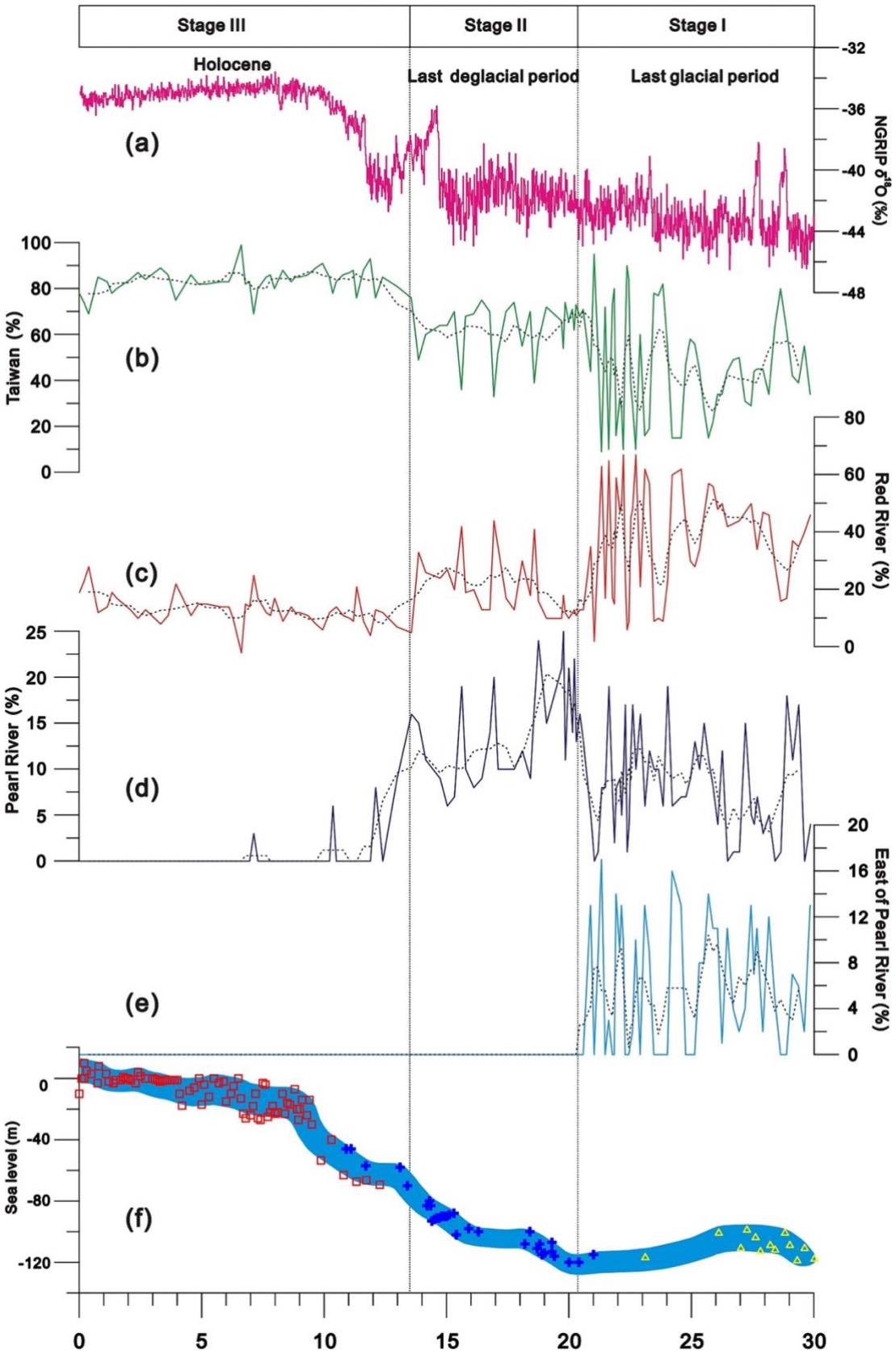

Figure 7 Comparison of the relative contributions from (b) Taiwan, (c) the Red River, (d) the Pearl River and (e) the area east of the Pearl River to sediments in the core XT-1, with (a) the $\delta^{18}O$ data from the Greenland ice core NGRIP (Rasmussen et al., 2006) and (f) sea level fluctuations over the last ~30ka. The dashed black curved lines in Figures 7b-8e present the running average values. Sea level data are sourced from Siddall et al., (2003) (red squares), Hanebuth et al., (2000) (blue crosses), and Grant et al., (2014).

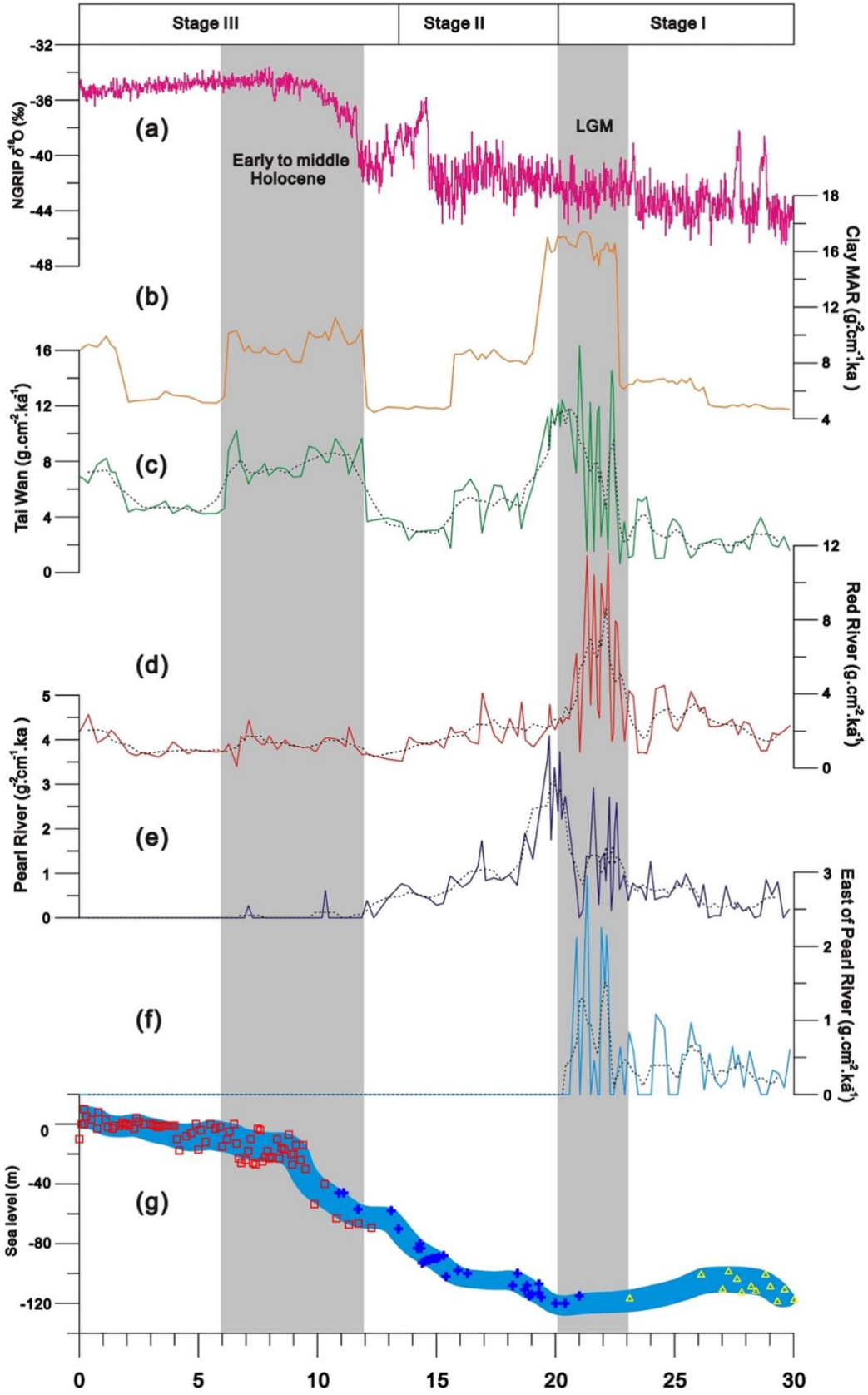

Figure 8 Temporal changes in (a) the $\delta^{18}O$ data from the Greenland ice core NGRIP (Rasmussen et al., 2006), (b) The clay MAR Taiwan, the MARs of clay sediments from (c) Taiwan, (d) the Red River, (e) the Pearl River, (f) the area east of the Pearl River, and (g) sea level. The gray shaded bars represent the LGM and the early to middle Holocene respectively, during which the flux of Taiwanese sediment notably

increased. The dashed curved lines in Figures 8c-8f indicate running average values. Sea level data are from Siddall et al., (2003) (red squares), Hanebuth et al., (2000) (blue crosses), and Grant et al., (2014) (yellow triangles).